N 65 - 33969

FACILITY FORM 602

(ACCESSION NUMBER)   (THRU)

91

(PAGES)   (CODE)

89

(NASA CR OR TMX OR AD NUMBER)

MELPAR INC

A SUBSIDIARY OF WESTINGHOUSE AIR BRAKE COMPANY

3000 ARLINGTON BOULEVARD, FALLS CHURCH, VIRGINIA

Table III

INDUCTOR VALUES

Substrate	Conductor width (mils)	Space (mils)	Outer diameter (inches)	Inner diameter (inches)
1	10	10	0.4	0
2	25	25	0.8	0
3	35	15	0.8	0
4	15	35	0.8	0
5	10	10	0.6	0

Substrate	Theoretical L(μh)	f_o(mc)	Actual L(μh)	f_o(mc)	Q (30 mc)	$\dfrac{f_o \text{ actual}}{f_o \text{ theoretical}}$
1A	0.392	168	0.498	86	4.3	0.52
1B	0.392	168	0.487	86.8	8	0.52
2A	0.544	105	0.555	77.7	6.9	0.74
2B	0.544	105	0.602	74.7	11.5	0.71
3A	0.544	105	0.527	79	8	0.75
3B	0.544	105	0.569	76.9	12	0.73
4A	0.544	105	0.615	75.2	5	0.72
4B	0.544	105	0.664	71.7	9.2	0.68
5A	1.15	74.5	1.47	49.8	5	0.67
5B	1.15	74.5	1.56	48.2	6.4	0.65

A = Corning 0211 glass substrate.

B = Englehard quartz substrate.

no apparent difference. The overiding factor seems to be the length of the coil conductor. To increase the self-resonant frequency, the spacing between conductors will be narrowed and the coil conductor length shortened.

6.5.3 Inductor, Q, Values

The dc resistance of the coils on 0211 glass was 0.025 ohm per square. This could be improved by a factor of 2.5 since 0.01 ohm per square is achievable. This, of course, means the Qs could have been 2.5 times greater. The Qs obtained on the quartz substrate were slightly greater since, on the first substrates, the resistivity of the two depositions (horizontal and vertical conductors) was different and, therefore, an attempt was made to keep the resistivity of the coil uniform throughout its length.

The resistance of the coils was measured as a function of frequency, and the resistance increased due to the skin-effect phenomenon. The skin depth for conduction at 30 megacycles is approximately 12,000 agnstroms. Since the films are approximately 25,000 angstroms thick, the radio frequency resistance begins to affect the Qs at 30 megacycles.

6.6 Conclusions

A coil of approximately 1.5 microhenries with a Q of 30 at 30 megacycles seems presently feasible in an area of 0.36 square inch and is capable of being formed with the same vacuum-deposition techniques and materials presently being employed in monotronic circuitry.

The self-resonant frequency of these coils is possibly satsifactory for intermediate-frequency use at 30 megacycles. However, the approaches previously discussed will be attempted to increase the self-resonant frequency to as high a value as possible.

The use of thick copper for 0.01 ohm per square seems to just allow for usable Q values. The surface area of the conductors must be kept as large as possible to minimize the skin effect.

7. HIGH-MAGNETIC-PERMEABILITY FILMS

7.1 Introduction

The investigations of high-permeability materials in thin-film form are in the early stages. The initial efforts are directed toward the goal of fabricating thin-film ferrites by standard vacuum-deposition techniques completely in vacuo. The present techniques of forming this ferrite films are by the vapor deposition of the metal, or mixed metals for bimetallic or tri-metallic compositions, in a) partial pressures of oxygen, or b) as metal films for postoxidiation in air or oxygen atmospheres.[29,30] The Method employed here to vacuum deposit Fe_3O_4 material in a vacuum of $1x10^{-5}$ torr has shown some degree of success. The method is to mix a small percentage of a stable and low-melting-temperature oxide (B_2O_3) with the Fe_3O_4 powder. When this mixture is deposited from a tungsten boat on a substrate at elevated temperatures, the resulting film exhibits some degree of magnetite structure. The data relating some of the physical properties of the films to the deposition parameters will be discussed.

7.2 Film Structure of Vacuum-Deposited Fe_3O_4-B_2O_3 Mixtures

7.2.1 Deposition Technique

The results of the Physical Electronics Laboratory in vacuum depositing electrically stable rare-earth borosilicate thin-film capacitors from metal boats[31] indicated that a similar technique could be applied to the vacuum deposition of iron oxides. Therefore, Fe_3O_4 (magnetite) was mixed with varying percentages of B_2O_3 powder and deposited from a tungsten boat in pressures of about $1x10^{-5}$ torr. It will be noted here that the vacuum-deposition techniques used throughout this phase are standard, and

normal operational procedures were used. Fused-silica substrates were used for the preliminary investigations.

It was found that film resulting from a Fe_3O_4-B_2O_3 mixture of 95%-5% by weight was optimum. A larger ratio of B_2O_3 resulted in films that were hydroscopic and light in color, whereas a lesser ratio of B_2O_3 resulted in films that were reduced metal (or nearly so). Most of the films deposited were of the 95%-5% mixture.

To obtain initial results relating to iron-oxide films, a reduced film deposited from a 99%-1% mixture was heated in air at $1200^\circ C$ for 2 hours and rapidly quenched in ice water. The X-ray diffraction pattern of the reduced film showed the Fe line at $d = 2.00\overset{\circ}{A}$. The oxidized and quenched film ex-hibited a predominantly red color with some degree of black appearance and the X-ray diffraction pattern is shown in figure 23. The pattern did not show elemental iron, and the results are given in table IV and compared with ASTM index cards. It was found that α- Fe_2O_3 (rhombohedral structure) and γ-Fe_2O_3 (tetragonal structure) were present. Several lines not agreeing with the known lines were present, but it is postulated that source im-purities are responsible as it will be pointed out later.

The films that were deposited on a substrate at 200° to $400^\circ C$ did not exhibit diffraction lines. This indicated that the film was either amorphous or consisted of extremely small crystallites. The films that were deposited on the substrates at 200°-$400^\circ C$ and annealed in situ in the vacuum of 1×10^{-5} torr in a temperature range of 550° to $750^\circ C$ did exhibit crystalline structure. The X-ray diffraction lines of the Fe_3O_4 powder, and of the films annealed for 15 minutes in vacuum at $520^\circ C$, $650^\circ C$, and $750^\circ C$, are shown in figures

2θ = 24.9 d = 3.57

2θ = 22.5 d = 3.95

2θ = 33.8 d = 2.65 Å
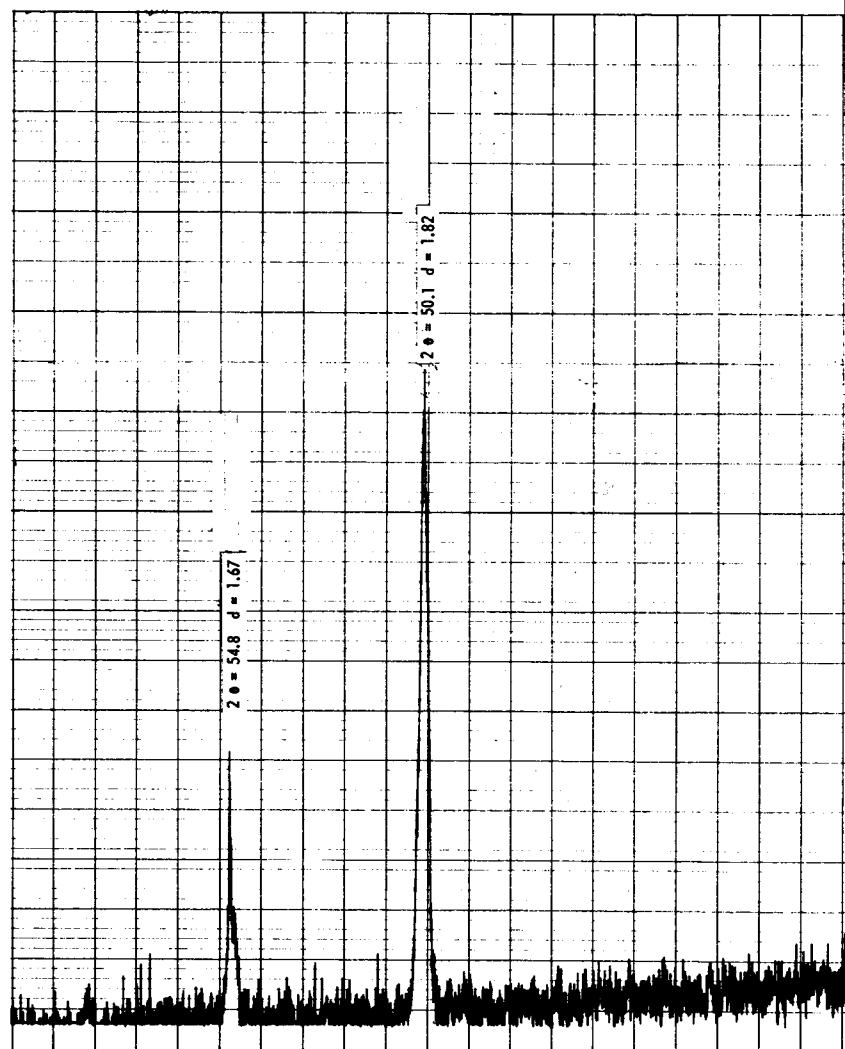
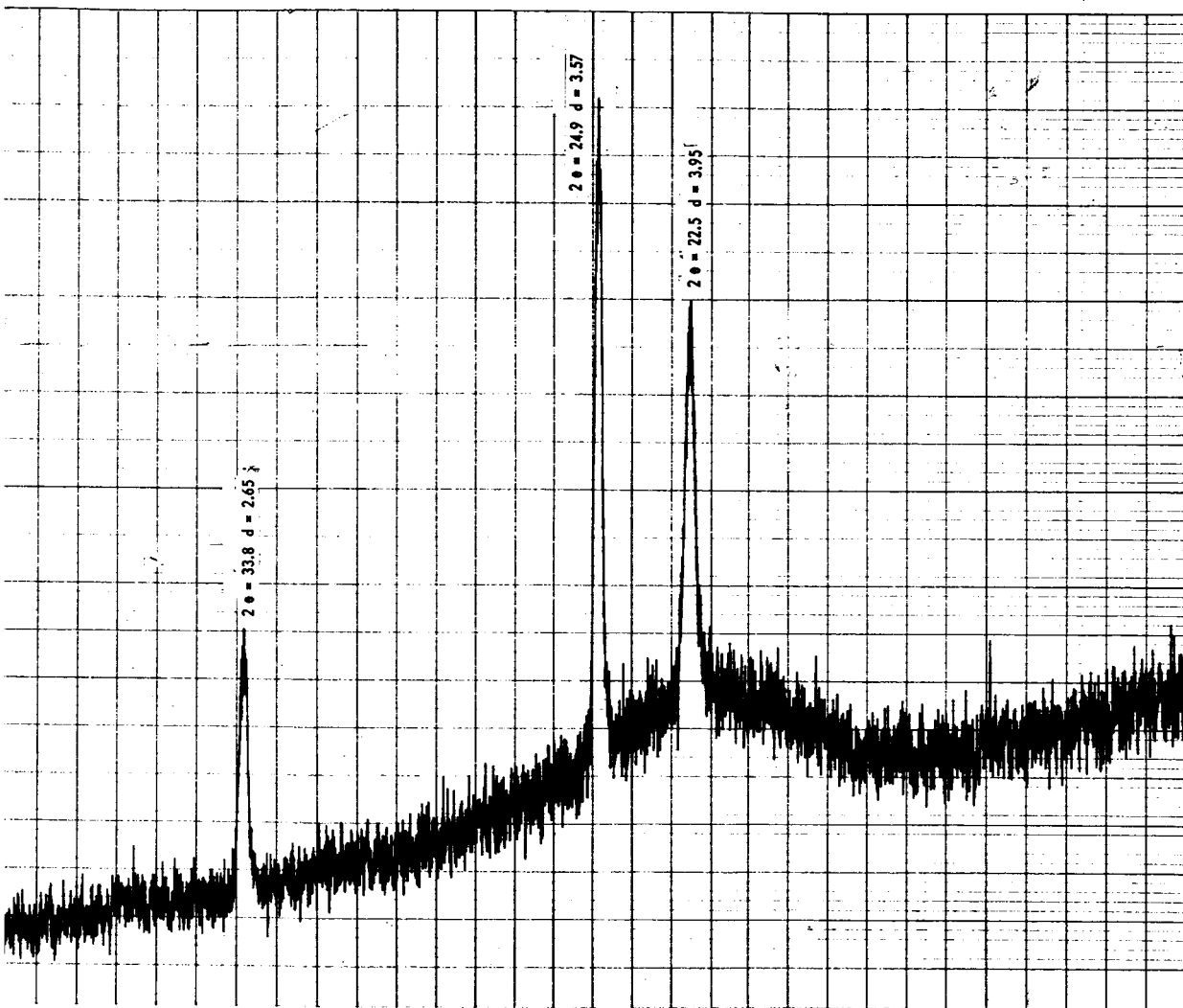Figure 23. X-ray Diffraction Pattern of Oxidized Fe Film

75

Table IV

COMPARATIVE X-RAY DATA OF OXIDIZED AND QUENCHED Fe FILMS

Film #9A

$d, \overset{o}{A}$ (exp)	I/I_o (Rel)	α-Fe$_2$O$_3$ (ASTM) Rhombohedral $d, \overset{o}{A}$	I/I_o	hkl	γ-Fe$_2$O$_3$ (ASTM) Tetragonal $d, \overset{o}{A}$	I/I_o	hkl
3.95*	S				3.72	M	210
3.57*	S				3.398	M	213
2.65	M	2.69	S	104	2.634	W	310
1.82	S	1.838	M	024	1.81	S	423
1.67	M	1.69	M	116	1.699	M	426
1.52	W				1.52	W	523

Note:

S, Strong intensity

M, Medium intensity

W, Weak intensity

*, Lines not identified.

24, 25, 26, and 27 respectively. The lines are tabulated and compared with the ASTM lines shown in table V. The film annealed at $520^{\circ}C$ showed a slight crystal structure, and the film that was annealed at $650^{\circ}C$ exhibited lines that agreed with the magnitite lines. The film annealed at $750^{\circ}C$ exhibited magnitite lines, but also lines that have not been studied for identification.

The accuracy of the lines determined by the X-ray diffraction patterns does not show complete agreement with the ASTM lines, or even with the lines from the Fe_3O_4 powder. Variations have determined to be $\pm0.06\overset{o}{A}$ in determining the d lines. Some of the error is due to instrumentation error, but the largest errors are due to line broadening and slight displacement of the lines due to impurities in the Fe_3O_4 powder. However, the lines corresponding to magnitite Fe_3O_4 are present; thus, the preliminary results indicate the technique of mixed source materials $(Fe_3O_4+B_2O_3)$ may be satisfactory for vacuum deposition of ferrites.

7.3 Chemical Analyses

The source material of Fe_3O_4 was analyzed for cation impurity. The material obtained from Fisher Scientific Co., Purified, was not certified and other sources are being sought for greater purity. However, the X-ray diffraction data of the powder (see table V) showed several unidentified lines. The chemical analyses of the Fe_3O_4 powder are compared with the deposited film and are shown in table VI.

It is interesting to note that the added B_2O_3 in the mixture did not increase the concentration in the film over the initial amount of boron in the stock material. There was no increase of Cr and Mg, but an increase was noted for Al,Ca,Co, Ni, and Sn from the powder to the film composition.
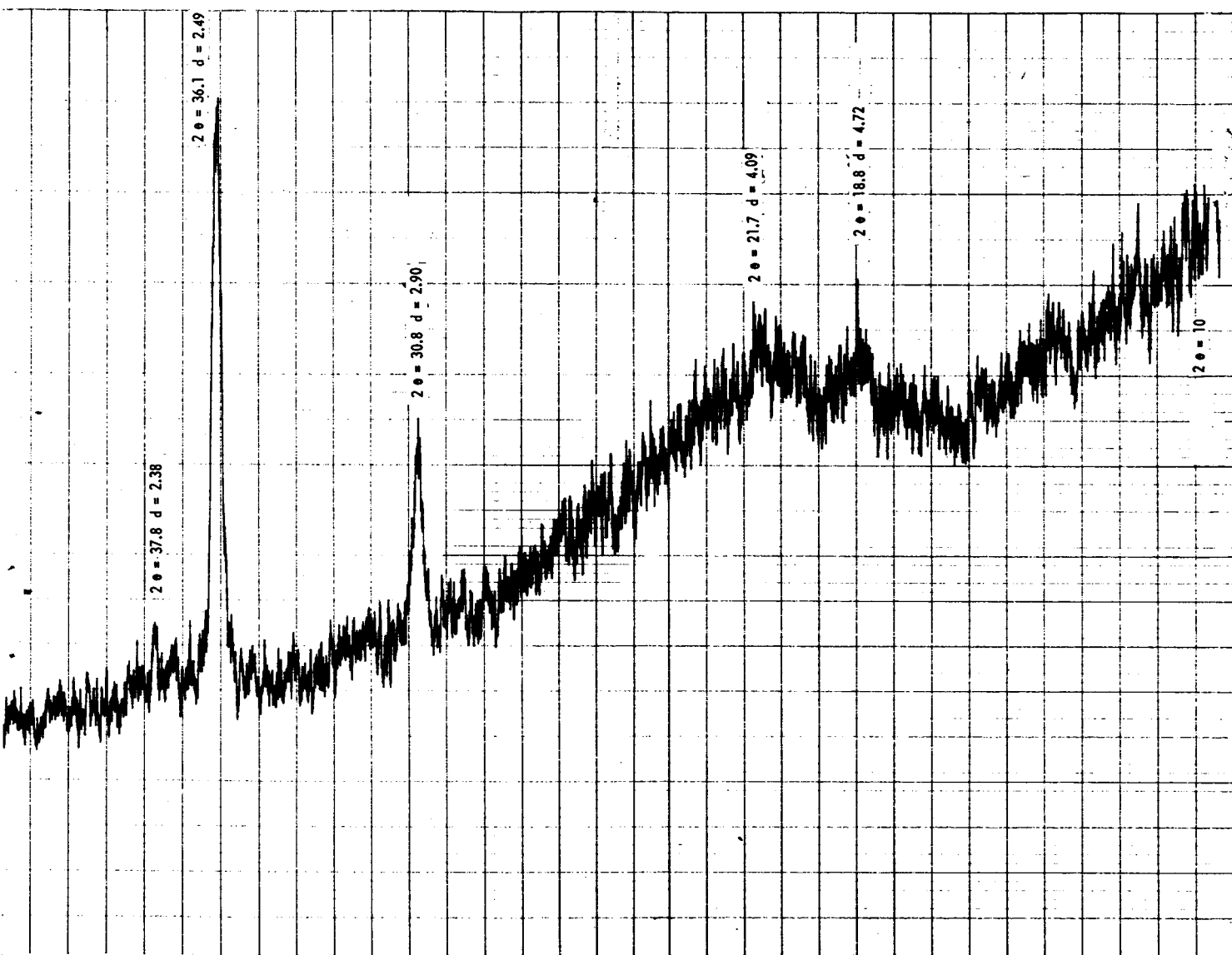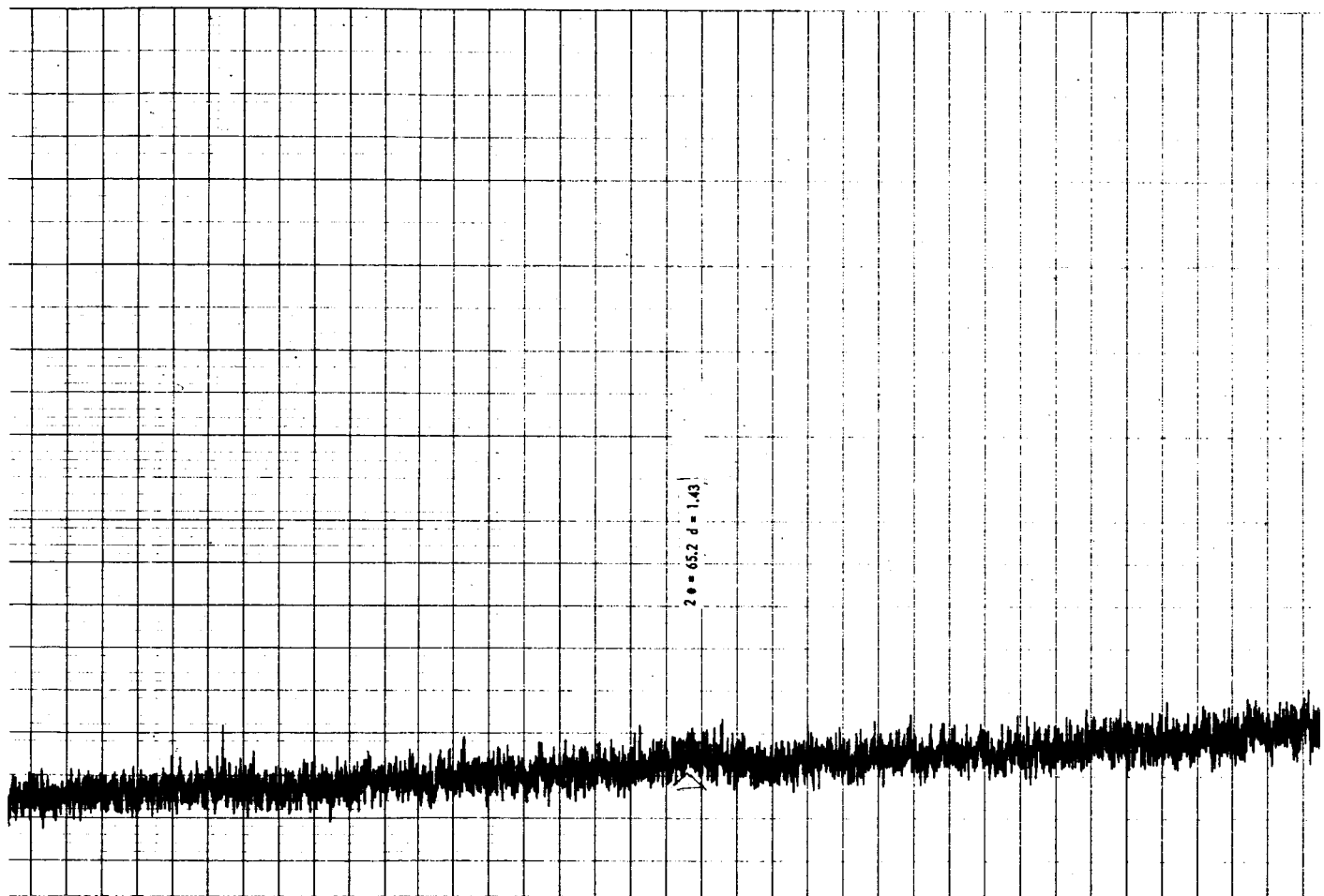
E19.34
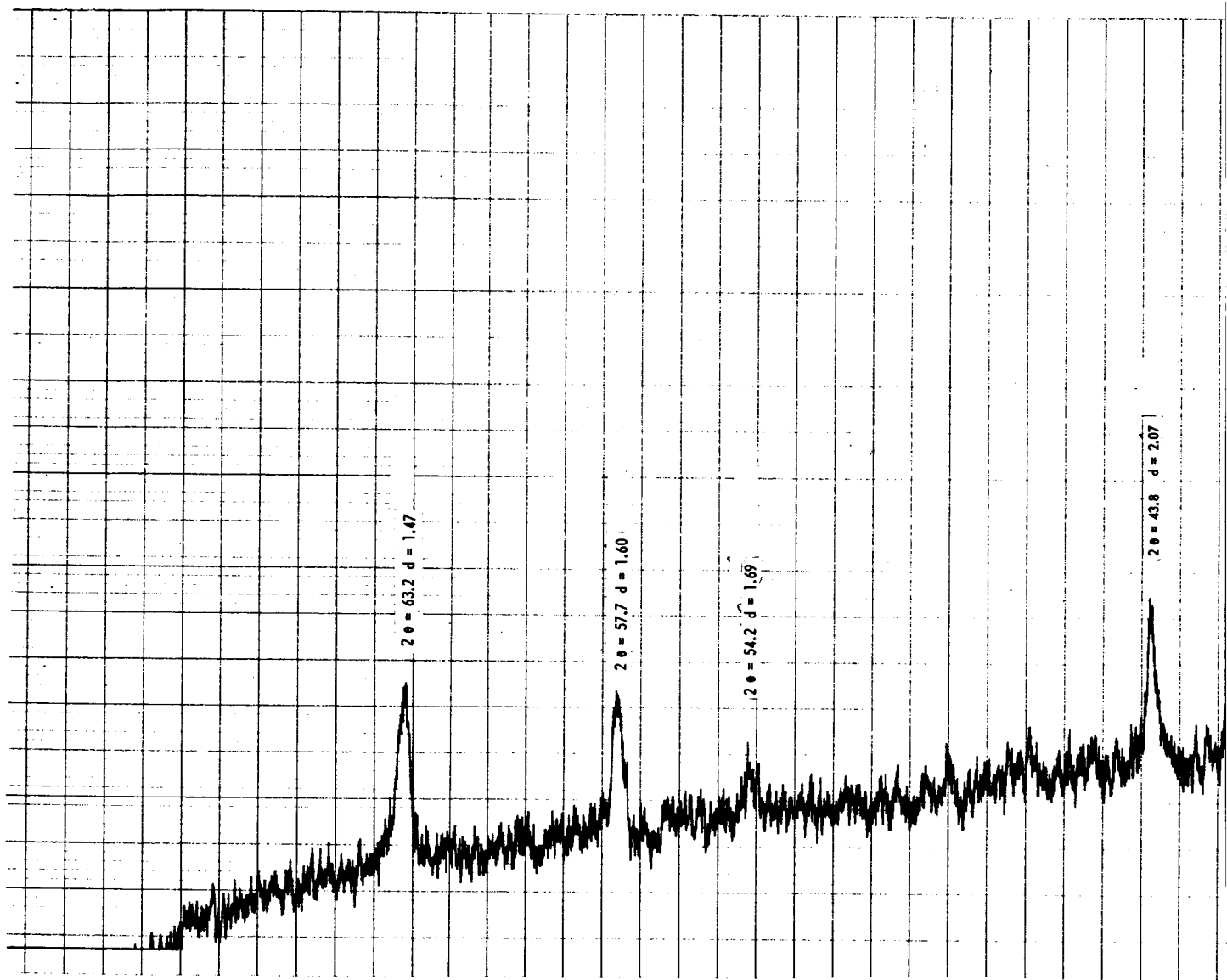
Figure 24. X-ray Diffraction Pattern of Fe_3O_4 Powder

E1935

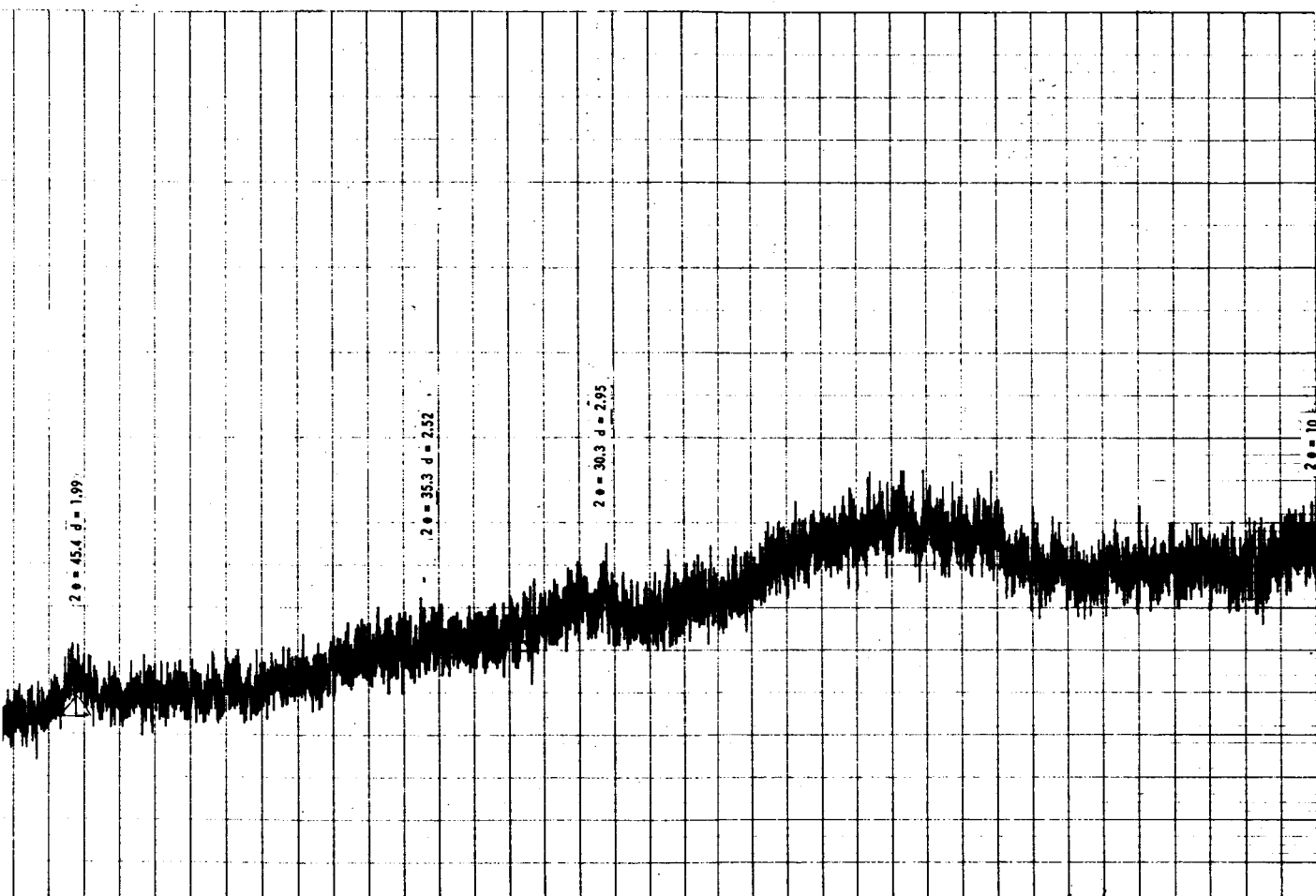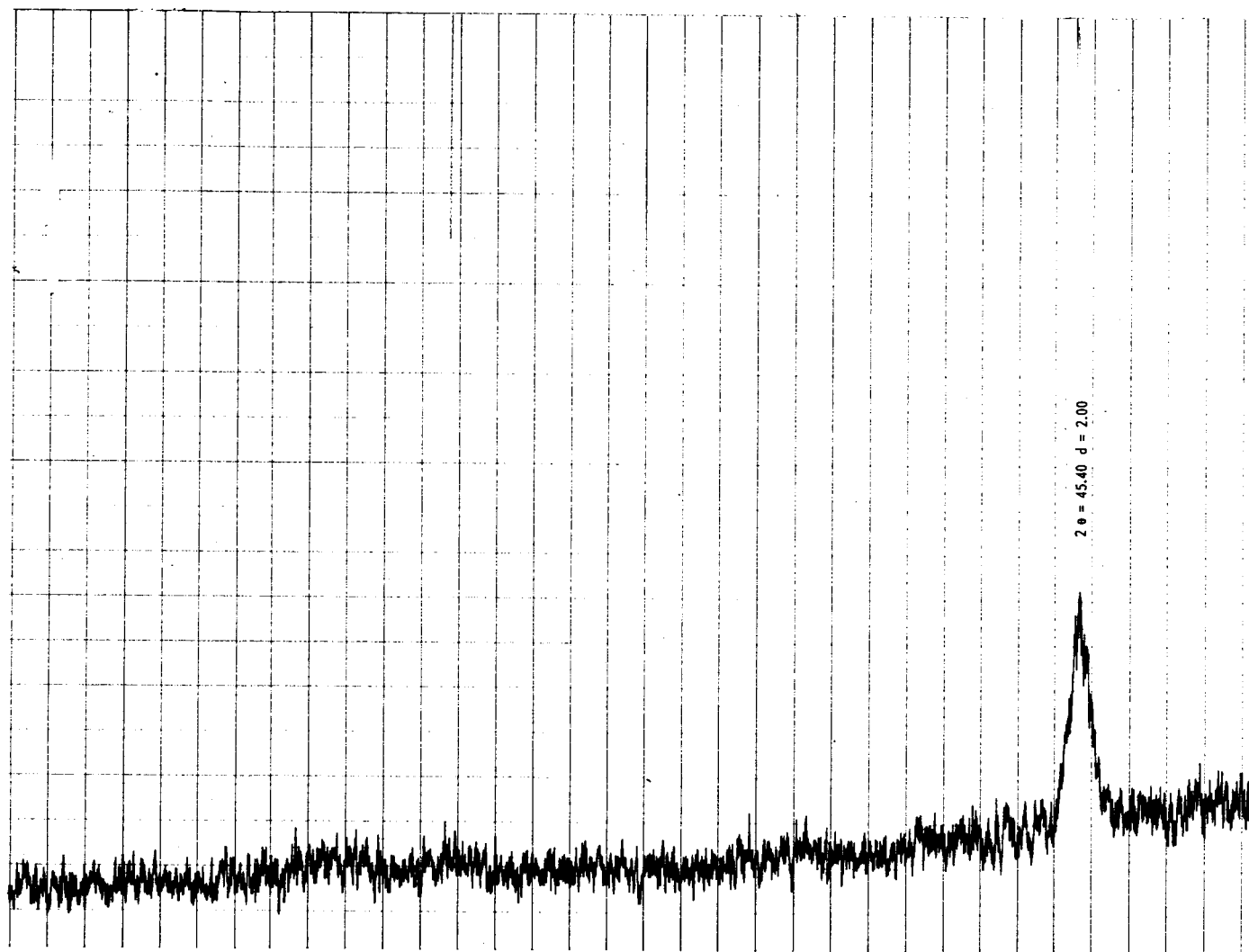2 θ = 65.2 d = 1.43

Figure 25. X-ray Diffraction Pattern of Fe_3O_4-B_2O_3 Film Annealed at $520^{\circ}C$
for 15 Minutes

E1936

2 θ = 45.40 d = 2.00
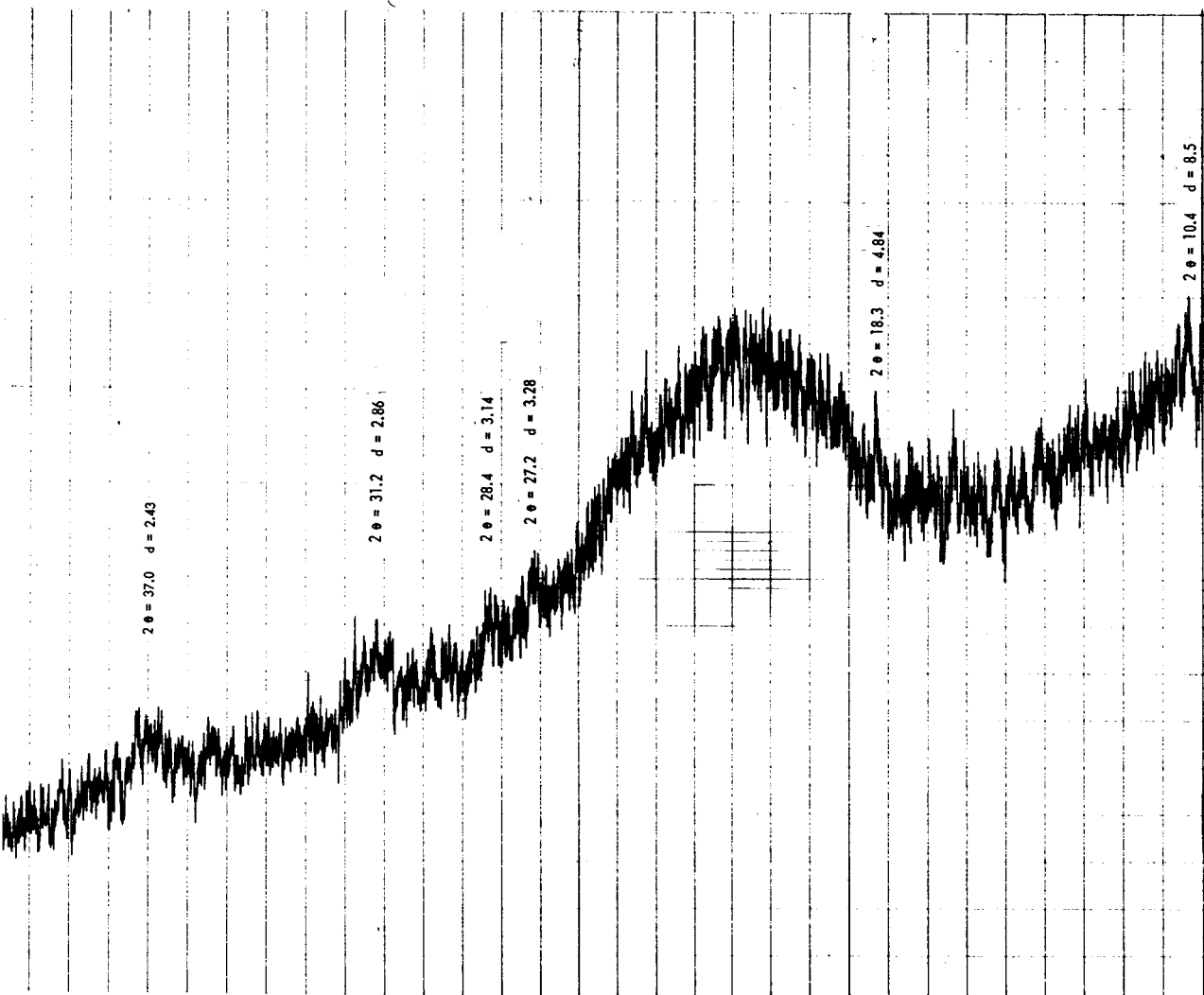
Figure 26. X-ray Diffraction Pattern of Fe_3O_4-B_2O_3 Film Annealed at 650^oC for 15 Minutes

E1937
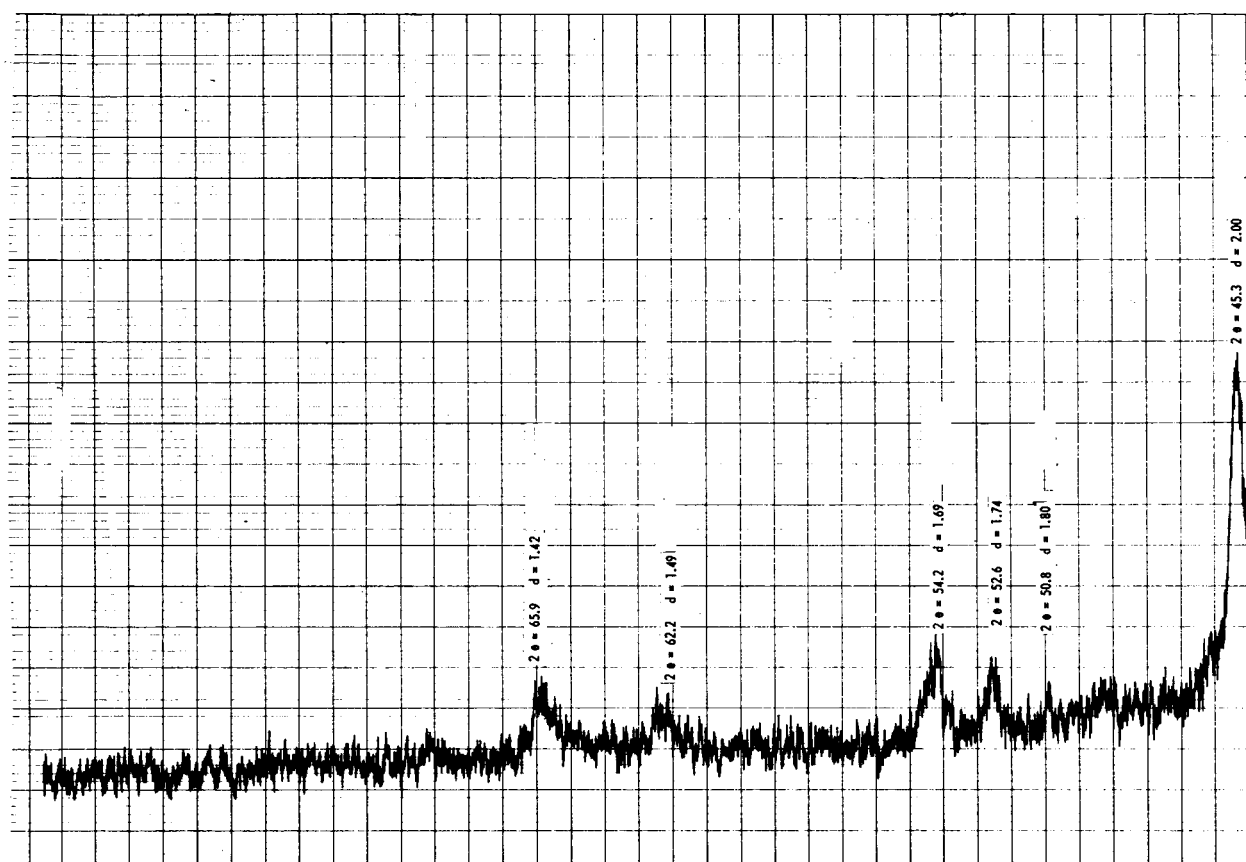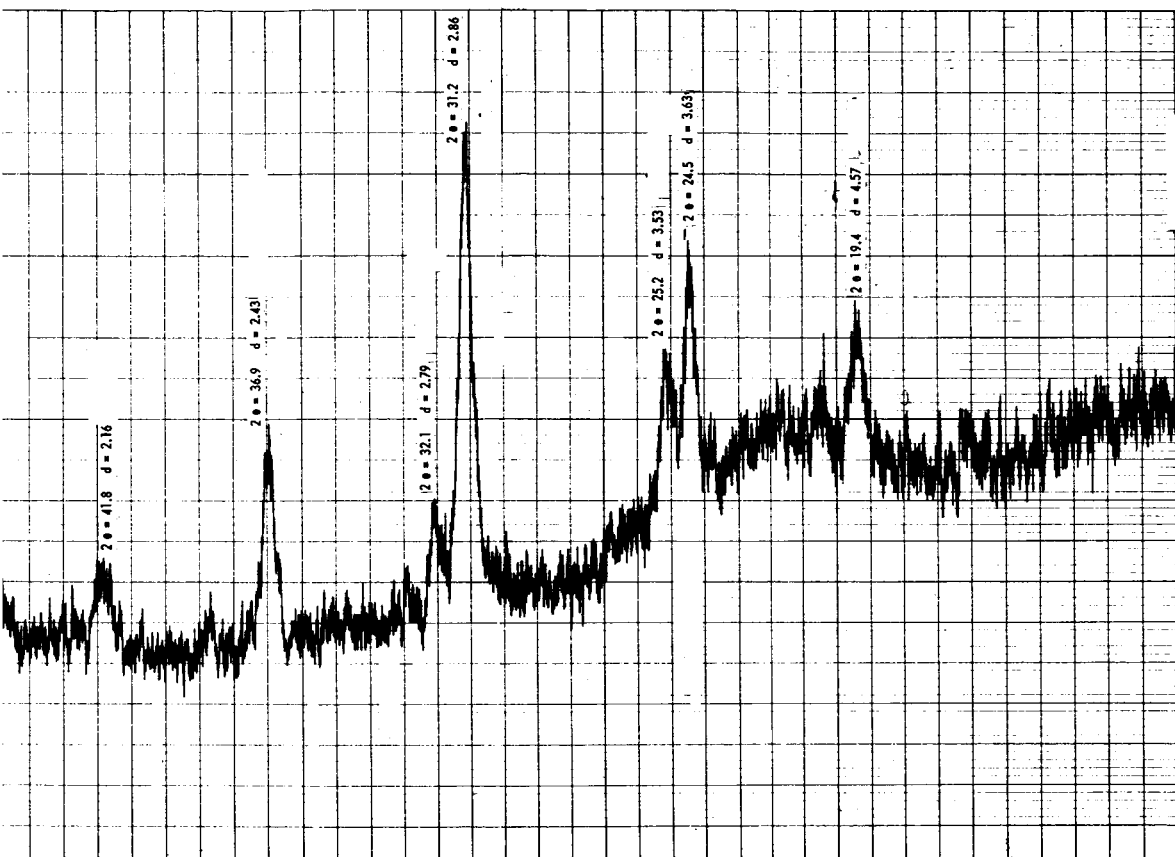
Figure 27. X-ray Diffraction Pattern of Fe_3O_4-B_2O_3 Film Annealed at 750°C for 15 Minutes

Table V

COMPARATIVE X-RAY DATA ON Fe_3O_4 MATERIALS IN VARIOUS FORMS

Fe_3O_4 Powder		Fe_3O_4 (ASTM) Magnitite, Cubic			Film #10 520°C Anneal		Film #12 650°C Anneal		Film #13 750°C Anneal	
d,Å (exp)	I/I$_o$ (Rel)	d,Å	I/I$_o$ (Rel)	hkl	d,Å (exp)	I/I$_o$ (Rel)	d,Å (exp)	I/I$_o$ (Rel)	d,Å (exp)	I/I$_o$ (Rel)
4.72	W	4.85	W	111			4.85	W	4.57*	W
4.09	W						3.28*	W	3.63*	M
							3.14*	W	3.53*	W
2.90	M	2.966	S	220	2.95	W	2.86	M	2.86	S
									2.79*	W
2.49	S	2.53	S	311	2.52	W	2.43	M	2.43	M
									2.16*	W
2.07	M	2.096	S	400	1.99	W	2.00	S	2.00	S
									1.80*	W
1.69	W	1.712	M	422					1.74	W
1.60	W	1.614	S	333 511					1.69	W
1.47	M	1.48	S	440					1.49	W
					1.43*	W			1.42*	W

Note:

S - Strong intensity

M - Medium intensity

W - Weak intensity

* - Lines not identified.

Table VI

CHEMICAL ANALYSES OF Fe_3O_4 POWDER AND FILM

Element	Fe_3O_4 Powder	Fe_3O_4 Film
Al	FT	W
B	W	W
Ca	FT	W
Cr	W	W
Co	FT	S
Fe	VS	VS
Mg	W	W
Ni	FT	S
Sn	X	FT
W	X	X

Note: Concentration

FT	0.001-0.005%
T	0.005-0.01%
W	0.01-0.5%
M	0.5-4.0%
S	Major component
VS	Major component
X	Searched, but not detected.

The Co and Ni are major components with Fe. This means that the film may be a mixture of magnitite and bimetallic and trimetallic ferrites. Thus, more detailed study of the films is required.

An important result shown in table VI is that tungsten was specifically sought since it was the crubible material. The results were negative, which meant that the mixture of Fe_3O_4 and B_2O_3 was unaffected by tungsten. A tantalum crucible reduced the mixtures and was dissolved by the molten iron.

7.4 Electric and Magnetic Properties of Vacuum-deposited Fe_3O_4-B_2O_3 Mixtures

The electrical magnetic properties of the vacuum-deposited films of the Fe_3O_4-B_2O_3 mixtures were investigated to a limited extent. The reason was that the main effort during the first quarter was to do a literature search on the methods of previous methods of forming thin-film ferrites, and then to apply the capabilities of Melpar for the vacuum deposition of Jerril films per se.

The films were deposited in a configuration of 2 cm on an edge, i.e., an area of 4 cm^2. The resistances of the films should be related to the film composition and structure. However, the exactness of the relationship cannot be ascertained because of the impurity concentration deviations from stiochiometry and degree of crystallinity. The resistivity of the films was measured in ohms/sq. The results are shown in table VII. The preliminary indications do not warrant postulating an optimum annealing temperature and source mixture. These conditions cannot be optimized unitl Fe_3O_4 of higher purity can be obtained. Howsver, initial results indicate that a 1-5% B_2O_3 to 99-95% Fe_3O_4 mixture annealed at $650°C$ appears to be optimum.

Table VII

RESISTIVITY IN Ω/sq OF FERRITE FILMS

Film No.	Composition starting material	Resistivity Ω/sq	Remarks
5-B	Fe_3O_4	65	Metallic appearance
6-B	$10\% B_2O_3 + 90\% Fe_3O_4$	10^{10}	Translucent light brown color
7-B	$5\% B_2O_3 + 95\% Ee_3O_4$	1.5×10^8	Dark color
8-B	$5\% B_2O_3 + 95\% Fe_3O_4$	4×10^7	Dark color; annealed at 400°C
9-A	$1\% B_2O_3 + 99\% Fe_3O_4$	10^3	Slight metallic appearance
9-B	$1\% B_2O_3 + 99\% Fe_3O_4$	---	Oxidized in air 2 hours at 1200°C, predominately red color
10-B	$5\% B_2O_3 + 95\% Fe_3O_4$	6×10^3	Dark color; annealed at 520°C
11-B	$5\% B_2O_3 + 95\% Fe_3O_4$	1×10^4	Dark color; annealed at 650°C
12-B	$1\% B_2O_3 + 95\% Fe_3O_4$	50	Dark color; annealed at 650°C
13-B	$5\% B_2O_3 + 95\% Fe_3O_4$	35	Dark color; annealed at 750°C

(All annealing time -- 15 min in vacuum)

The films were not measured for specific magnetic properties such as permeability, saturation magnetization, coercive force, etc. The reason was that the equipment was not available for such measurements. The most available method for determining if the films exhibit magnetic properties was to utilize the results on the inductor patterns. (See section 6.)

An inductor pattern on a fused-silica substrate had a "Q" of 18 at 60 mc with a capacitance of 11.2 pf. The "Q" was 18.2 at 70 mc with a capacitance of 7.6 pf. This inductor pattern had a 5% B_2O_3- 95% Fe_3O_4 deposited to 5000Å thick and annealed at $600^{\circ}C$. The "Q" of the sample at 70 mc was 11 with a capacitance of 51.8 pf. At 60 mc, the "Q" was 10 with a capacitance of 70.5 pf. The increased capacitance was due to the decrease of resistance of the inductor coil in contact with the ferrite film. Thus, the change of "Q" of the coil in this instance has not verified any ferromagnetism.

On a ferrite film that had been deposited and the "Q" measured. At 60 mc, the "Q" was 5.1 with a capacitance of 10.9 pf. Another ferrite film was deposited on the coil, i.e., the coil was sandwiched between the two ferrite films, and the "Q" remeasured. The value of "Q" was 11 at 60 mc with a capacitance of 51.8 pf. Thus, in this case, the "Q" was increased, however, sufficient data were not taken at this time for true evaluation of the inductor coil imbedded between the ferrite films, and to verify ferromagnetism.

7.5 Program for the Next Quarter

Sources of higher-purity Fe_3O_4 material are being sought for the deposition of the films. Emphasis will be placed on varying the deposition parameter for obtaining a higher degree of magnitite structure. X-ray

diffraction pattern, chemical analysis, and optical absorption curves will be obtained for film characterization.

A "B-H" looptracer is being acquired for observing the magnetization curve of the thin-film ferrites. The permeability, saturation magnetization, remnant magnetization, and coercive force of the films will be measured.

The resistivity of the films will be remeasured carefully to correlate the electrical properties of the films with the parameters of film formation.

8. CONCLUSIONS

All research in the specified areas is on or ahead of the planned schedule. The efforts expended in the practical investigations of substrates, dielectrics, and inductors are yielding definite information for high-frequency calculations. The most important research area, high-frequency thin-film triodes, has had the design approaches well defined, and intensive research experiments are being carried out. The research into magnetic permeability films is also defined and being investigated. It is in the area of the alternate metal base device that advances beyond the existing state of the art have been achieved so unexpectedly early in the program. Furthermore, detailed analysis is under way in this area to fully and completely define the operating mechanisms and the deposition parameters.

9. REFERENCES

1. J. Lilienfield, U.S.Pat. 1,745,175 Jan. 28, 1930; U.S.Pat. 1, 900,018 Mar. 7, 1933.

2. O. Heil, U.K. Pat. 439,457 Mar. 4, 1935.

3. W. Shockley and G.L. Pearson, Phys. Rev. 74, 232 (1948).

4. C. Feldman, Conf. on Navy Lab. Microelectronics, APL, Johns Hopkins University. June 12-13, 1961, OTS No. (PB -18134) p.53.

5. P.K. Weimer, IRE-AIEE Device Res. Conf. Stanford University, Stanford, Calif. June 26-28, 1961.

6. P.K. Weimer, Proc. IRE 50, 1462 (1962).

7. H. Wilson, W. Layton, W. Gutierrez, and C. Feldman, Electrochemical Soc. Spring Meeting, Pittsburgh, Pa. April 14-18, 1963.

8. H. Wilson and W. Gutierrez, Electrochemical Soc. Spring Meeting, Pittsburgh, Pa., April 14-18, 1963 (Late news article).

9. F. V. Shallcross, Proc. IRE 51, 851 (1963).

10. R. Zuleeg, Solid State Electronics, Vol. 6, p. 193, Mar., Apr. 1963.

11. J.E. Kauppila, Proc. IEEE, Vol. 51, p. 472, Mar. 1963.

12. P.K. Weimer, F.V. Shallcross, and H. Borkan, RCA Rev. 24, 661, (1963).

13. R. V. Shallcross, op. cit. 24, 676 (1963).

14. W.A. Gutierrez and H.L. Wilson, IEEE Trans, on Electron Devices ED-11, 466 (1964).

15. W.A. Gutierrez and H.L. Wilson, Proc. IEEE (Correspondence) Vol. 52, p. 607 (1964).

16. P.K. Weimer, Proc. IEEE (Correspondence) Vol. 52, p. 608 (1964).

17. W.A. Gutierrez and H.L. Wilson, Proc. IEEE (Correspondence) Vol. 53, p. 92 (1965).

18. H.L. Wilson and W.A. Gutierrez, Journal of the Electrochemical Soc., Vol. 112, p. 85-91 (1965).

19. Electronics, Mar. 8, 1965 p. 149.

20. First Quarterly Report on Field Effect and Space Charge-Limited Thin-Film Triodes. DA36-039-AMC-02374, U.S. Army Electronics Material Agency, RCA (1963).

21. M.M. Atalla and R.W. Soshea: Solid State Electronics, $\underline{6}$ (1963)245.

22. M.M. Atalla and D. Kohng, "A New Hot Electron Triode Structure", presented at the Solid State Devices Research Conference, Durham, New Hampshire, July 9-11, 1962.

23. W. Spitzer, C. Crowell, and M.M. Atalla, Phys. Rev. Lett., Vol. 8, pp. 57-58; January 1962.

24. H.H. Skilling, Electric Transmission Lines, McGraw-Hill, 1951, p. 15.

25. Ibid., p. 21.

26. H.E. Bryan, "Printed Inductors and Capacitors," Tele-Tech 14, No. 12, December 1955, p. 68.

27. J.M.C. Dukes, Printed Circuits, MacDonald, London, 1961.

28. H.H. Skilling, Fundamentals of Electric Waves, Second Edition, John Wiley and Sons Inc., New York, 1948.

29. E. Banks, N.H. Riederman, H.W. Schleunering, and L.M. Silber, "Formation and Study of Thin Ferrite Films," Symposium of American Vacuum Society, 1960, Pergamon Press, New York, pp. 297-305.

30. L.M. Silber, "Variation of the Magnetization of Thin Nickel Ferrite Films with Thickness," Studies in Microwave Physics, Final Report No. PIBMRI - 12 41-64 (1964), pp. 13-39.

31. M. Hacskaylo and R.C. Smith, "Electrical Properties of Dysprosium Borosilicate Thin-Film Capacitors," Submitted to J. Electrochemical Society.

Senior personnel who participated in work on this contract this quarter are:

Dr. Charles Feldman

Mr. William A. Gutierrez

Mr. Michael Hacskaylo

Mr. J. Howard Hoskinson

Mr. Richard C. Smith

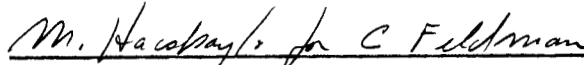Mr. Wendell Spence

Mr. Herbert L. Wilson
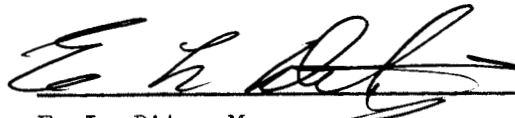
Mr. Barry J. Weiner

Prepared by: _____
Barry J. Weiner
Liaison Project Engineer

Approved by: _____
Charles Feldman, Manager
Physical Electronics Laboratory

_____
E. L. Ditz, Manager
Space Research and Technology Center

_____
Paul E. Ritt, Vice President
Research and Engineering

First Quarterly Report

THIN-FILM PERSONAL COMMUNICATIONS
AND TELEMETRY SYSTEM (TFPCTS)

For the period of December 21, 1964 to
March 21, 1965

Contract No. NAS 9-3924

April 1965

Submitted to

National Aeronautics and Space Administration
Manned Spacecraft Center
Houston, Texas

Submitted by

Melpar, Inc.
3000 Arlington Boulevard
Falls Church, Virginia

TABLE OF CONTENTS

LIST OF ILLUSTRATIONS

LIST OF TABLES

1. INTRODUCTION

The First Quarterly Report is submitted in compliance with Contract NAS 9-3924. Phase A of this contract is a research effort to develop thin-film active devices and passive circuit elements for use at ultrahigh frequencies. These thin-film components are for the design of a Thin-Film Personal Communications and Telemetry System (TFPCTS) in monotronic form.

The work effort and time schedule, as delineated on the PERT Chart for Phase A in the TFPCTS Addendum, serve as a guide line for the research required in this contract. It must be realized, however, that in a research effort such as this, it is difficult to define the tasks exactly since the possibility always exists for a branching development to present itself as a desirable alternate approach.

Upon award of the contract, personnel were assigned to each of the outlined tasks. At this time, there have been no unexpected problems, and work is progressing smoothly in accordance with the time schedule as discussed in the monthly letters.

The reports of progress achieved during this quarter are presented in each of the individual categories of the PERT Chart.

2. HIGH-FREQUENCY THIN-FILM TRIODES (FIELD EFFECT)

2.1 Introduction

Theory of operation, electrical characteristics, and materials for the thin-film transistor or thin-film triode (TFT) can be found in numerous articles. In view of substantial agreement of investigators and the considerable coverage given these devices, particularly during the past three years, a list of references is given in lieu of a lengthy review (See references 1-18).

For a point of clarity, the device referred to in this contract is an all-thin-film structure deposited by vacuum-deposition techniques on an amorphous substrate. The thin-film device can be described as a thin-film, field-effect, insulated gate transistor (or triode). Decision as to the term transistor or triode might be argued, but in lieu of discussion, the term TFT will be used in reports. It is further acknowledged that some might call the device a type of MOS transistor, however, we shall leave that term for devices formed by investigators on single-crystal substrates.

Figure 1 (a), (b), (c) represents three of the more basic TFT structures.

Weimer et al.[12] have identified the structures of figure 1(a) by the name "Staggerd," and the structure of figure 1(b) by the name "Coplanar." At the present time, no known identification has been assigned by investigators to the structure of figure 1(c). A tentative name of "Planar" is given at this time for future identification in these reports.

Basically, the phenomenon desired (transverse field effect) is to effect the conductance of the semiconductor layer between the source and drain electrodes via a transverse electric field placed on the insulated gate electrode. Elaboration is left to references cited.

STAGGERED

SOURCE (METAL)

GATE (METAL)

DIELECTRIC

SEMICONDUCTOR

DRAIN (METAL)

SUBSTRATE

(a)

COPLANAR

SOURCE (METAL)

GATE (METAL)

DIELECTRIC

SEMICONDUCTOR

DRAIN (METAL)

SUBSTRATE

(b)

PLANAR

SOURCE (METAL)

GATE (METAL)

DIELECTRIC

SEMICONDUCTOR

DRAIN (METAL)

SUBSTRATE

(c)
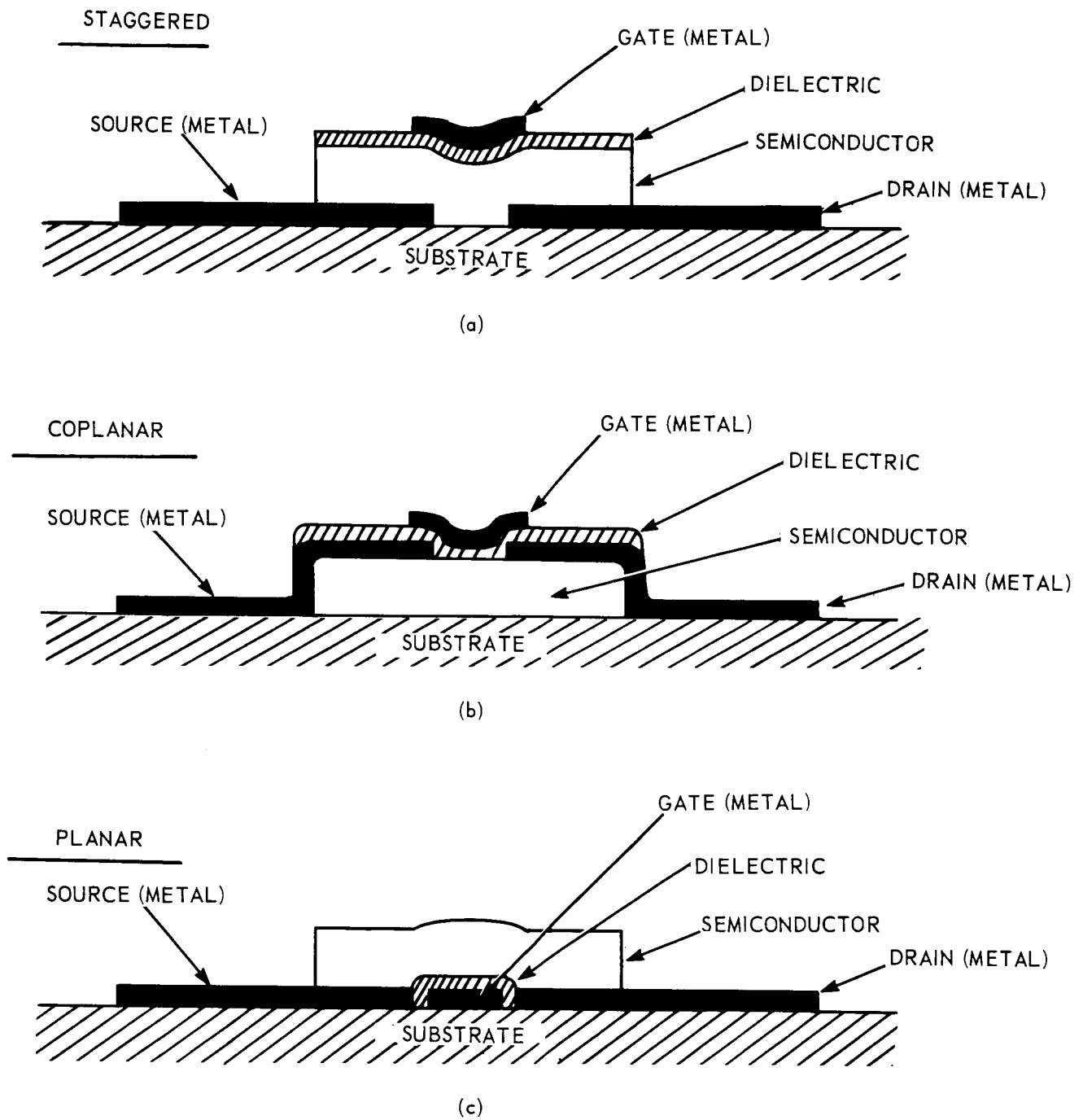
Figure 1. TFT Structures

Many variations of these structures have been proposed, or are bound to be. These variations follow, or will probably follow, four principal variations of the basic structures.

1. Reversal of film layer order.

2. Addition of two or more gate electrodes, or control electrodes, to further influence the semiconductor properties.

3. Insulated "grid-like" gate electrode, or electrodes, placed transverse to source-drain current flow.

4. Various geometric patterns of source-drain spacings. Device-structure variation, film-thickness variation, deposition-parameter variation, and choice of materials used in forming the thin-film device present a vast area of exploration before the investigator.

Various advantages of each of the three basic structures of figure 1(a), (b), (c) are immediately recognizable, or become apparent through theoretical study and device-forming practice.

Device parameters, however, are still largely dependent upon laboratory processes utilized, and apparent advantages of one structure over the other are not always realized in practice. A probable advantage of the "Planar" structure is that it is conducive to etching and anodizing techniques in forming the electrodes and dielectric insulation (i.e., Al_2O_3). Problems may arise, however, with the interference of the metal films on the semiconductor treatment, or the interaction between the dielectric and semiconductor layer during such treatment. A problem of ohmic contacts with the source and drain electrodes to the semiconductor may also arise.

A probable advantage of the "Coplanar" structure is that the semiconductor film can undergo sensitizing treatment free from the influence of metal layers. Low-temperature metals, such as In or Ga, may also be used for source-drain electrodes.

The greatest advantage of the "Staggerd" structure may be the ability of the investigator to utilize the dielectric layer to change the semiconductor surface to a sensitive, low-conductivity layer. This structure also seems to exhibit less problems with nonohmic and blocking contacts at the source and drain electrodes. Major problems of this structure include possible interference by the source-drain contacts during the semiconductor treatment and less precision in the spacing of electrodes.

Work this quarter has mainly utilized only the "Staggerd" structure of figure 1(a). The structures of figure 1(b) and figure 1(c) will be more thoroughly studied in following quarters.

2.2 Equipment Used for Forming TFTs

2.2.1 Environmental Control

Control of environment for laboratory facilities at the present time is one of temperature and air conditioning. Humidity, however, is not controlled. Work is now in progress to complete a "dry room" by April 15. This room will be maintained at a relative humidity of 25% or below. Two twin-vacuum systems (2-10 in bell jars per system) will be located in this area, principally for the purpose of forming TFTs. Formation of devices and protection in a lower humidity are expected to improve the stability and lifetime of these devices.

2.2.2 Vacuum Units

Although techniques for forming TFTs in a 24" bell jar system are now being investigated, devices at present are primarily formed in small 10" bell jar systems. A dual (twin 10") system is now being utilized, together with two single 10" systems. A second dual unit is presently under construction, with completion expected by April 15.

The two dual systems are expected to be the principal vacuum equipment used in future studies. These units exhibit relatively rapid pumping capabilities (10^{-6} torr in 5 minutes) with ultimate capability to 10^{-7} torr. Rapid pumping rates ensure good vacuum, 5×10^{-6} torr or better, during vaporization from relatively large charges of volatile materials (CdS, CdSe). Two filament transformers of up to 4000-watts capability are part of each dual unit. Two substrate heater supplies (Variac, 10-amp, 120-V capability) are also available on each dual unit. High-current feedthroughs are water cooled, and other standard features have also been included on these systems. Figure 2 is a photograph of the system interior and control panel of a small dual unit.

A small single (10" bell jar) vacuum unit is at present being used in the formation of Te devices. Use of Te in other units is being avoided at this time. This is being done for two reasons. Of the materials being investigated, Te is considered the most toxic or potentially dangerous to laboratory personnel. This vacuum unit, therefore, utilizes greater than normal precaution. The entire system is located in a hood enclosure of 1/8-inch plastic, and the roughing pump exhaust is enclosed in a second air-exhaust system. A second purpose of intentional Te deposition isolation at this time is based
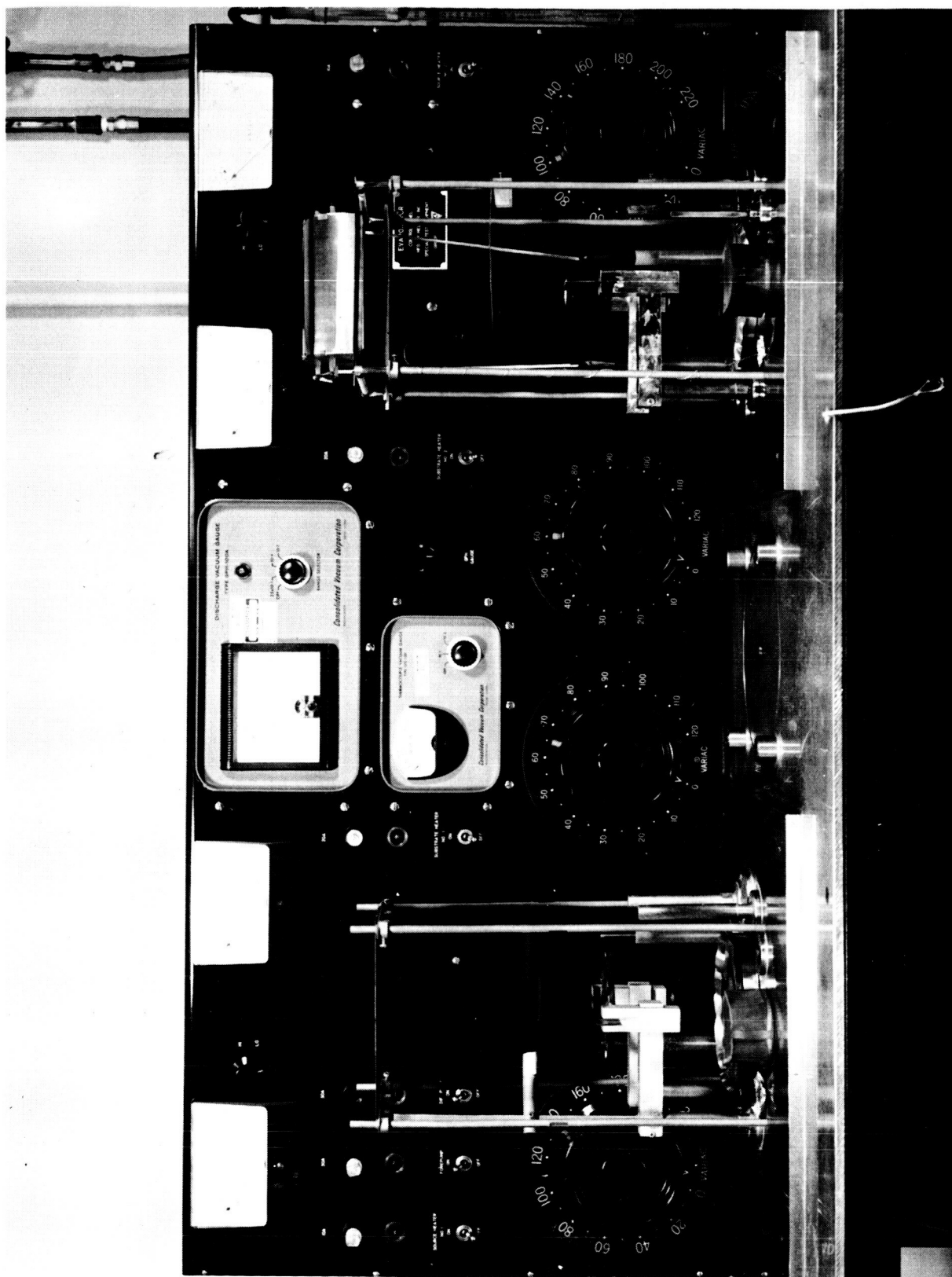
Figure 2. Interior and Control Panel of Small Dual-vacuum System

on private communications from two laboratories in which systems previously used in Te evaporations were found to be permanently unsatisfactory for latter attempts at forming hard nichrome films (in spite of careful and complete system cleaning.) At this time, this laboratory-cannot confirm this phenomenon. Films of various materials, including nichrome, have been deposited in the unit used for Te without apparent loss of normal film hardness. This was done, however, after the system had been cleaned, and where Te deposits had been made utilizing a pyrex chimney. The chimney restricted approximately 75% of extraneous deposit and was removed for other deposits (See figure 3). Precautions will continue next quarter.

2.2.3 <u>Characteristics Checkout Equipment</u>

Electrical parameters of the devices are studied on either a 570 (Tektronix) characteristic curve tracer or on a 575 (Tektronix) transistor curve tracer. Of these, the 575 is more versatile and is desired for observing "p" type device characteristics (i.e., Te). Addition of external bias (battery and pot arrangement) is required and, in the case of the 575, a 1K resistor permanently inserted between base and emitter jacks provides gate steps (step selector) in voltage levels as desired.

2.3 <u>Material Studies</u>

2.3.1 <u>Semiconductor Films</u>

To date, the most active TFTs (all thin film on amorphous substrates) have utilized either CdS, CdSe, CdTe, or Te for the semiconductor layer. (See references 1-18.) Other materials have been utilized, but thus far seem less sensitive either as to transconductance values or "pinch-off" (drain current saturation) capability.
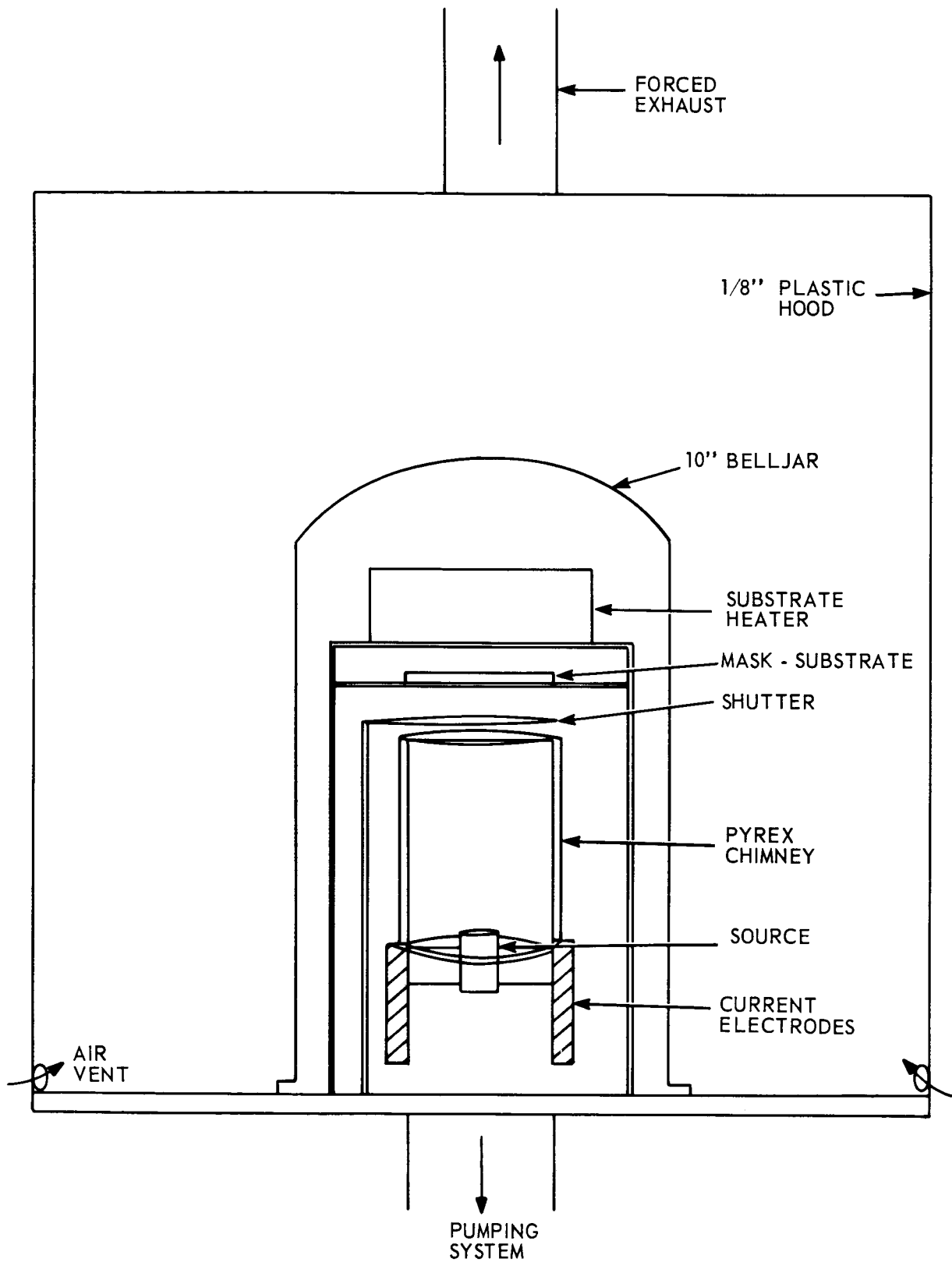
Figure 3. Enclosure and System Setup for Te Evaporations

This quarter, CdS, CdSe, CdS-CdSe, and Te films were investigated. Devices utilizing these films were formed and characteristics studied. CdS, CdSe, and CdS-CdSe (coevaporation of CdS and CdSe) films were "n" type. Te films were "p" type.

2.3.1.1 CdS: Cadmium sulfide (CdS) films were deposited using Eagle-Pitcher or Harshaw very-high-purity cadmium sulfide. The source material was ground to a fine powder. A charge of 4 grams was evenly dispersed on the bottom of a silicon dioxide crucible. To obtain a large surface-evaporation area, a 2-1/4-inch-diameter crucible (2-1/2 inches high) was used. For rapid heating and cooling, the SiO_2 crucible was inclosed at the bottom and sides with a tight-fitting tantalum (0.003") housing. Current was supplied to the housing, via 0.020" Ta ends, from heavy (water-cooled) copper electrodes. To prevent spitting, a low-density quartz wool blanket was placed over the source material.

Films were formed at rates from 50 to 100$\overset{o}{A}$ per second to thicknesses from 2500 to 5000$\overset{o}{A}$. Thickness buildup could be observed by visually observing color changes occurring on the freshly cleaned molybdenum mask. By observing and noting color and number of color cycles undergone in the film formation, a thickness to within 200$\overset{o}{A}$ could be predicted. Source temperatures ranged from 750° to 850°C in experiments of CdS deposition. Vacuum during depositions was in the vicinity of 5×10^{-6} to 10^{-6} torr. Deposition rates were not only dependent upon source temperature and vacuum, but also largely dependent upon evaporation area, source CdS particle size, and substrate temperature (source-to-substrate distance was held constant). A substrate temperature of 125°C was utilized.

Immediately after deposition, films were subjected to a heat treatment or anneal in vacuo (10^{-6} torr). This treatment was very short (2 minutes), in which a temperature of approximately 230°C was attained. After heating, the CdS films are allowed to cool to approximately 180°C (20 sec) and then the system is opened to air. Samples are removed while still warm and quenched to room temperature by placing them face up on a clean formica table top. Films were lemon yellow in color.

At room temperature, a dark resistivity in the vicintiy of 10^5 ohm/cm was exhibited. Deposition of an oxide dielectric, such as SiO, over the CdS film reduced the resistivity from 10^5 ohm/cm to as low as 10^2 ohm/cm. This drop is probably due to a number of actions resulting in oxygen removal from the CdS film surface. Removal of oxygen probably begins first by the reinsertion into vacuum for the SiO deposition, light and heat influences from the SiO source boat, bombardment of SiO molecules, and then most significantly by the gettering action of the SiO layer. This gettering action is attributed to an oxygen-deficient SiO layer containing elemental silicon attempting SiO formation or SiO attempting SiO_2 formation. Removal of the oxygen atoms (which at this time are believed to act as acceptors) results in increased conductivity.

2.3.1.2 CdSe: Cadmium selenide (CdSe) films were deposited from either sintered cake (Harshaw) or polycrystalline CdSe (Clevite) as the source material. The source material was ground to a fine powder. A charge of 4 grams of powder is placed in a graphite crucible of 1-and-1/4-inch diameter (0.050" wall). The charge of CdSe powder is then pressed to form a self-sustaining layer

approximately one-half way up the sides (1-and-1/4-inch high) and over the entire bottom of the crucible for a large evaporation surface. The graphite crucible is housed in a tantalum heater similar to the silicon dioxide crucible described in the CdS film formation. Similar rates, temperatures, and other deposition parameters resulted in CdSe films exhibiting resistivities before and after the deposition of an overlying SiO dielectric layer of approximately 1/10 of those observed for CdS layers. A problem of film-thickness monitoring is experienced with CdSe since color changes are not discernible. Monitoring of thickness during deposition was made by controlling time and source temperature, and by visual observance of film opaqueness by light transmission through the glass substrate exposed to deposition. Films were dark brown in color.

2.3.1.3 <u>CdS-CdSe</u>: Since it has been reported that photocells of Cds and CdSe mixtures exhibit the stability of CdS cells and the speed of CdSe cells[19] an attempt to study such layers for device application has been initiated. For these studies, compounds of the CdS-CdSe system were not used as the source material at this time, but rather a mixture of the two materials (1/1 by weight - 2 grams each). Evaporation was made from the silicon dioxide crucible arrangement in the manner described for CdS. Films were glossy pink to red and exhibited resistivities before and after dielectric deposition somewhat higher (2 to 15 times) than CdS films. This was not expected, and in view of the few runs made thus far, conclusions as to relative resistivity (compared to CdS and CdSe) will not be made at this time.

2.3.1.4 <u>Te</u>: Tellurium deposits are made from relatively small charges (50 mg). A crucible of intermetallic compound (National Carbon Co.) was

primarily used. This crucible was fitted into a tantalum housing, as were the crucibles used in CdSe and CdS depositions. It was somewhat smaller in size (1/2-inch diameter and 1 inch in length). Several other crucibles, including quartz, were also found to work just as well.

Deposition rate of the Te was about $100\overset{o}{A}$ per second. Since device requirements were $200\text{-}300\overset{o}{A}$, a critical shuttering time (1 to 5 sec) was necessary. The deposit time was initiated with the appearance of Te on the chimney.

Deposits were made on the glass substrates with nichrome source-drain electrodes. An outgassing of the substrates in vacuum to $400^{\circ}C$ preceded a cooling to $50^{\circ}C$ or lower, at which temperature the deposition was made. At substrate temperatures above $125^{\circ}C$, deposits of Te would not occur.

2.4 High-mobility, Semiconductor Film Studies

In view of the high-frequency requirements of this contract, an additional investigation of materials exhibiting higher mobility than CdS, CdSe, CdS-CdSe, or Te has been initiated to include film-property studies of films of materials (primarily tellurides) in which high mobilities have been observed, and to form and investigate TFT structures utilizing these films. Presently being investigated are AgTe films. Mobilities of $400 \text{ cm}^2/\text{VS}$ have been noted for films of $2000\overset{o}{A}$ thickness. Due to the large carrier concentration, however, it appears that films below $400\overset{o}{A}$ in thickness will be required for TFT structures.

2.5 Dielectric Films

Investigation of oxide dielectrics such as SiO, SiO_2, La_2O_3, YB_2O_3, Nd_2O_3, Dy_2O_3, and B_2O_3 indicates that films of most oxide materials deposited by proper vacuum techniques may be satisfactorily utilized as the insulation

layer in TFT devices. Fluoride dielectrics as well as sulfides or certain elemental dielectrics might also be utilized. However, since oxygen absorption by the dielectric from the semiconductor surface is desirable, oxide dielectric layers will be concentrated on during the program.

During this quarter, SiO was primarily utilized as the insulator layer. For the "Staggerd" structure, an increase in conductivity of "n" type semiconductor layers was noted upon the deposition of SiO. (This is the case when oxide dielectrics are used and, to a lesser extent, when flourides are utilized.) An increase of semiconductor conductivity of up to 10^4 has been observed. Another method of increasing "n" type semiconductor conductivity is by heating the structure at room atmosphere in the temperature range of $400°$ to $600°C$ for a few minutes. This latter treatment is at present not utilized at Melpar for "Staggerd" structures in which oxide dielectrics are used.

Deposition rates for dielectrics vary from $6000\overset{o}{A}$ per minute for SiO down to $200\overset{o}{A}$ per minute for Dy_2O_3. Thickness monitoring of SiO is done usually by observing color change. A thickness to within $100\overset{o}{A}$ may be controlled in this manner. For dielectrics requiring high source temperature in which color change is less reliable, the amount of charge, source temperature, and time are used to control thickness.

2.6 Metal Electrode Films

Experience has indicated that aluminum is one of the most preferable metals for the gate electrode. As in regular thin-film capacitors, the self-heating properties of aluminum (i.e., the greater likelihood of pinhole oxidation) make this material popular. It is of relatively high conductivity and,

in the case of the "Planar" structure, the anodizing or oxidizing treatment of the gate electrode surface to form a grown oxide insulation presents a favorable technique. At the present time, aluminum is being utilized at Melpar for the reasons stated above.

Source and drain electrodes present a requirement of using a metal which forms an ohmic contact to the semiconductor film. Aluminum would be desirable from the standpoint of utilizing a single material for both source-drain electrodes and the gate electrode. It would be very desirable for some structures, like the "Planar" arrangement, where all electrodes might be deposited at the same time. The problem thus far, however, is that an oxidation or reaction at the aluminum-semiconductor interface often results in a high-resistance contact or blocking contact at either the source or drain electrode, or both. Most investigators have found gold to form a barrier with the "n"-type semiconductors of the type investigated here. Indium, gallium, or other such low-temperature materials probably cannot be used in the "Staggerd" of "Planar" structures because of the temperatures used in the semiconductor film formation.

In general, a low-work-function metal would be desirable in attempting ohmic contacts to "n"-type semiconductors and a high-work-function metal for contact to "p"-type semiconductor layers.

It has been observed at Melpar that nichrome (if exposure to air occurs between the source-drain deposition and the semiconductor deposition), without exception, resulted in as low and usually lower resistance contact to semiconductor layers being studied (n or p) as did any other metal.

It is believed this is due to the hardness of the layer, where slight chemical reaction of the metal-semiconductor interface reduces the barrier

expected, and to the formation of a more oxide-free metal surface. Chrome exhibits a similar characteristic if exposure to air does not occur between the metallic and semiconductor layer depositions.

For this quarter, nichrome was utilized for source-drain electrodes exclusively in the "Staggerd" structure. Aluminum was used on occasion in the "Coplanar" structure.

Deposition rates on the order of $2000\text{\AA}$ per minute were used in forming nichrome source-drain electrodes at a substrate temperature of 250°C for the "Staggerd" units. Aluminum gates for the various structures were deposited at a rate of $1000\text{\AA}$ per minute on a substrate of 50°C or lower.

2.7 <u>Masks</u>

Figure 4 shows the most basic TFT mask layout utilized. This layout configuration is used for 5- and 14-device arrangements per substrate. Four 1-inch-square substrates are used in the depositions. The actual device area used is small compared to substrate dimensions. For ease in handling in basic studies, however, the 1-inch-square substrates are used. Somewhat greater device density may be achieved with the 50-device arrangement (25 pairs - common source) of figure 5. The latter configuration or one of similar, yet higher, density arrangements is anticipated later in the program.

Mask No. 1 of figure 4 will have a tungsten wire attached after the basic mask is etched. This tungsten wire, down to 2.5 microns, is attached directly to the mask to form the closely spaced source-drain electrodes. The split gate pickup tab is used later as a visual guide in alignment of the gate electrode. This alignment (gate electrode to source-drain spacing) is done visually with the aid of light and magnification.

NOTE: ALL MASKS MADE FROM
5 MIL THICK MOLY EXCEPT
MASK NO. 4 WHICH IS 2 MIL

SCALE 20/1

0.005

MASK NO. 3
DIELECTRIC

MASK NO. 4 (GATE)
2 MIL WIDTH

MASK NO. 2
SEMICONDUCTOR

MASK NO. 5
PICKUP
CONDUCTORS

MASK NO. 1
SOURCE-DRAIN ELECTRODES
& GATE PICKUP

NEXT PATTERN LOCATION
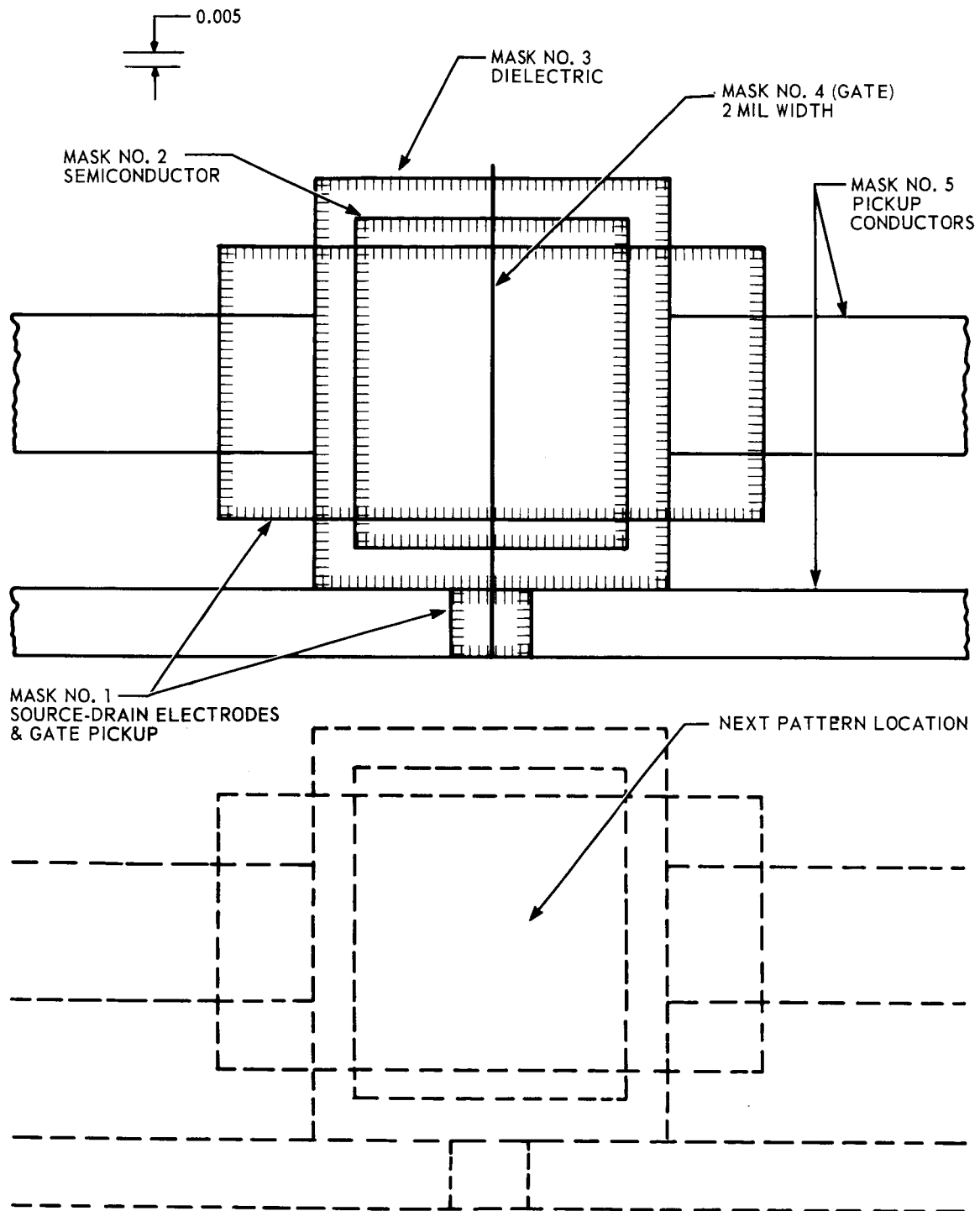
Figure 4. Basic TFT Mask Layout
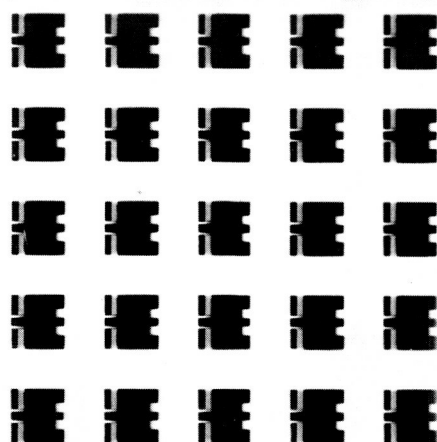
Figure 5. Common Source Arrangement of 25 TFT Pairs

The gate width used at this time (shown as 2 mils) will eventually be used as a base mask for a still-smaller opening. Techniques for obtaining 5-micron-wide gates are now being developed.

2.8 Substrates

Substrates presently being used are glass, one inch square. The type of glass being utilized in the initial investigations is Corning 0211 micro-sheet. Devices have been successfully deposited on 10- and 20-mil-thick substrates of this material. Other glasses (types 7052 and 7056 Kovar sealing glass) are reported to be preferred by other investigators.[20] This glass, however, is not known to be available in sheet form. Substrates of this material, therefore, would probably be obtained by cutting from rods and then using lapping and polishing techniques for obtaining substrates. Since it may be necessary to use a different substrate composition for high-frequency (300-mc) devices, no decision has been made yet to investigate 7052 or 7056 glass.

Corning 7059 glass is advertized as having properties which have merited investigation. TFTs were formed on this glass during this quarter, however the "pinch-off" characteristics have been disappointing thus far. This glass is also available only in 30-mil thickness, a factor which must be considered in weight and space requirements of this contract.

Substrates used are cleaned by standard ultrasonic cleaning procedures. They are also outgassed in vacuum (10^{-6} torr) at a temperature of $400°C$ prior to source-drain and semiconductor depositions for 5 minutes.

Glow discharge cleaning was not utilized in any cleaning or film-forming depositions this quarter.

2.9 Source Heaters

Figure 6 shows typical source-material heaters used in the formation of TFTs. The heater at the top of the photograph is a type used in the semiconductor evaporation. A graphite, quartz, or any other type crucible is press fitted into the tantalum housing shown. The middle heater is the standard 10-mil (commercial) tungsten boat. It is used for all metallic depositions. Such boats are good for up to 40 aluminum evaporations, but only for six michrome depostions.

The bottom heater is used for SiO and some other relatively low-temperature depositions. Its shape is such to engulf the area of the mask and substrate. This is believed to minimize shadowing and pin holes of the dielectric layer. It also provides a very even deposition for relatively short source-to-substrate distances. This boat is shaped from 10-mil tantalum.

2.10 Substrate Heater

Figure 7 shows a bottom view of the type of substrate heater used. This heater is capable of heating lightweight mask-substrate assemblies to $800^{\circ}C$. The heater has a 10-mil tantalum frame with a removable 3-mil tantalum reflector. Heat is supplied by three 500-watt, quartz (G.E.), infrared lamps.

2.11 TFT Characteristics

Figure 8 shows characteristics of a CdSe TFT formed this quarter. SiO was used as the dielectric. Film thickness for the CdSe and SiO layers were 5000Å and 1100Å respectively. Nichrome source-drain electrodes (1000Å) were utilized with a 500Å-thick aluminum gate electrode. The device was of the "Staggerd" structure.

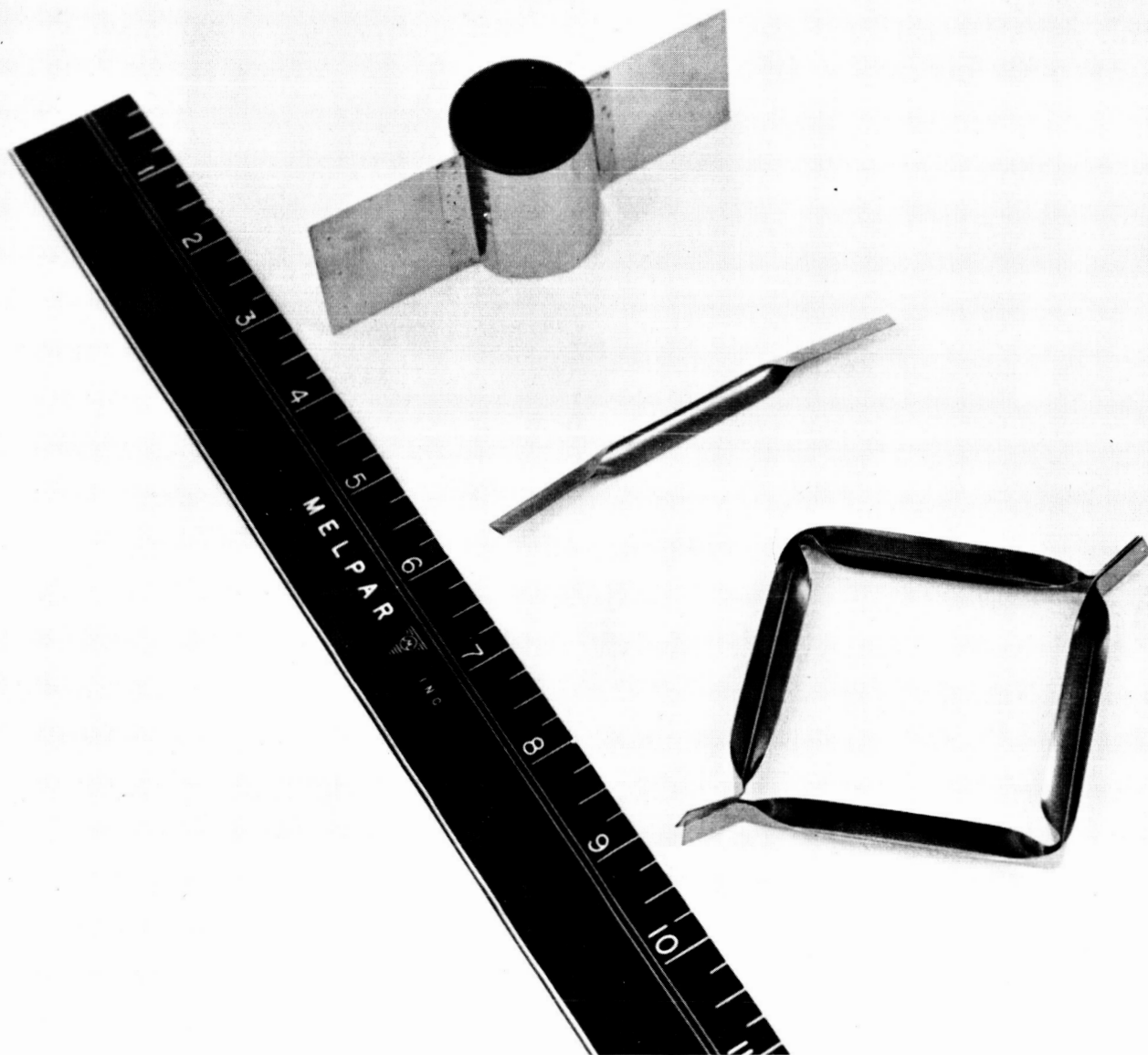Figure 6. Source Heaters Used for Evaporations
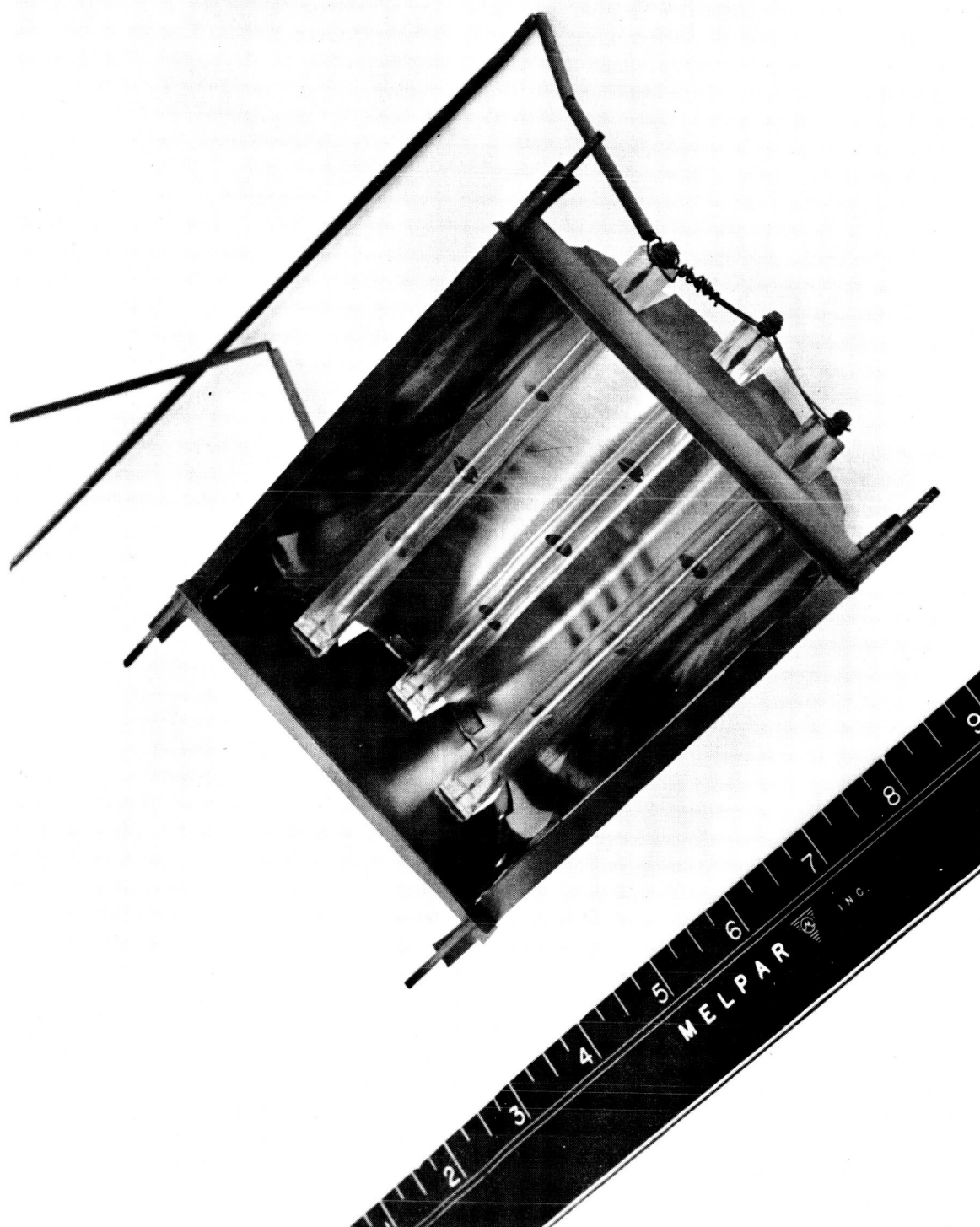
Figure 7. Substrate Heater Used for All Evaporations Requiring Substrate
Heating

2.0 ma

Id

Eg
+8.2 V

RL = 1 K
gm = 1200 µ mhos

+6

0   Vd   10
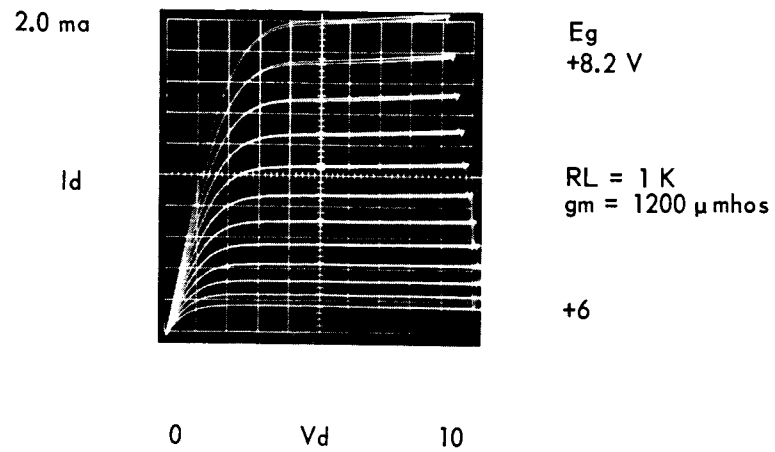
Figure 8. Characteristics of CdSe TFT

0.5 ma

Id

Eg
+6V

RL = 500 Ω
gm = 100 µ mhos

0

0   Vd   20 V
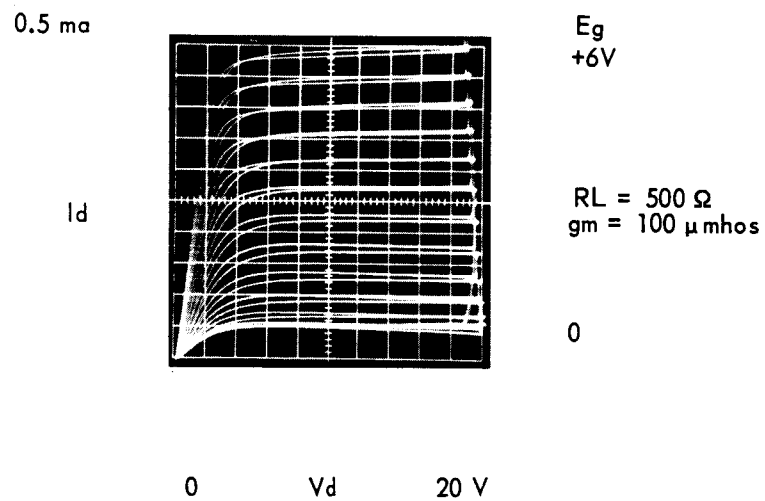
Figure 9. Characteristics of CdS TFT

Characteristics of a CdS device are shown in figure 9. As in the case of the CdSe device, SiO is used as the dielectric. Film thickness for the CdS and SiO layers were 3500Å and 1200Å respectively. This device exhibited rather small transconductance, but could stand relatively large gate and drain voltages without breakdown. Drain voltages to 30 volts could be used before breakdown or zener characteristics began to appear.

Characteristics of CdS-CdSe mixture devices are not shown. Generally, they were the same as those shown for the CdS device, however, transconductance values of the relatively few devices investigated thus far have been below 100 μ mhos.

Characteristics of a Te device formed this quarter are shown in figure 10.

2.12 Summary of TFT Investigations This Quarter

The first half of this quarter was heavily committed to designing and forming masks, building a second dual-vacuum unit, and ordering materials.

Source-drain spacings of 2.5 microns, utilizing 2.5-micron tungsten wire, were achieved this quarter. This spacing presents little problem. Achieving comparable gate widths is a greater problem and will be concentrated on during the next quarter.

Transconductance values of CdS and CdS-CdSe mixtures were low in devices formed this quarter, however, they appear promising for future device formation. CdSe devices (with which Melpar has more experience) have been formed exhibiting transconductance value to 5000μ mhos and power capabilities in excess of 100 MW.
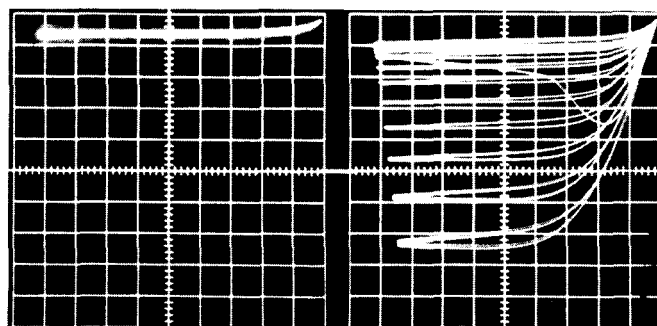
VERTICAL   0.02 ma/div
HORIZ.   1V/div
GATE V - 0.1V/STEP
ZERO BIAS - SHOWN ON LEFT
RL = 1K OHM

Figure 10. Characteristics of Te TFT

3. METAL BASE TRANSISTOR

3.1 Introduction

A class of solid-state devices known as "hot electron devices" gives promise of a method for achieving an ultrahigh-frequency thin-film amplifier. One such device is the metal base transistor (MBT), [21, 22] which consists of a thin metal film (100-700Å) sandwiched between two "n" type semiconductors. This metallic base layer is made thinnner than the mean free path of electrons and is accordingly transparent for injected electrons.

Figures 11 and 12 show the structure and energy band diagram of the MBT. The operation of the device can be followed with the aid of figure 12. The barriers formed at the metal-semiconductor interfaces are those studied by Schottky. The biased energy diagram in figure 12 shows that a forward bias applied to the emitter interface decreases the barrier height and correspondingly increases the number of electrons that are injected into the base region by flowing over the emitter potential barrier. These injected electrons are very energetic (or hot) since they possess energy greater than the Fermi energy in the metal. The hot electrons that are transported across the "transparent" metal base are then collected by passing over a lower-energy base-collector barrier into the space-charge region of the reverse-biased collector. The control of the current flow from one semiconductor (emitter) to the other (collector) is exercised by varying the emitter barrier height by means of the metal base layer.

The advantages of the MBT as an approach to an ultrahigh-frequency thin-film aplifier become apparent if one considers its frequency performance and unipolar operation.

METAL (COLLECTOR CONTACT)

N-TYPE SEMICONDUCTOR
(COLLECTOR)

THIN METAL (BASE)

N-TYPE SEMICONDUCTOR
(EMITTER)

METAL (EMITTER CONTACT)
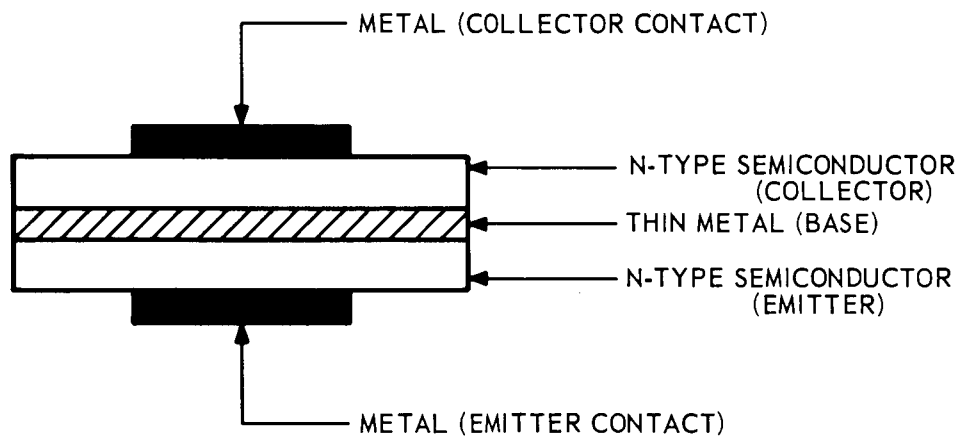
Figure 11. Structure of Metal Base Transistor

N-TYPE
SEMICONDUCTOR
(EMITTER)

METAL
(BASE)

N-TYPE
SEMICONDUCTOR
(COLLECTOR)

(a)

(b)

$q V_c$
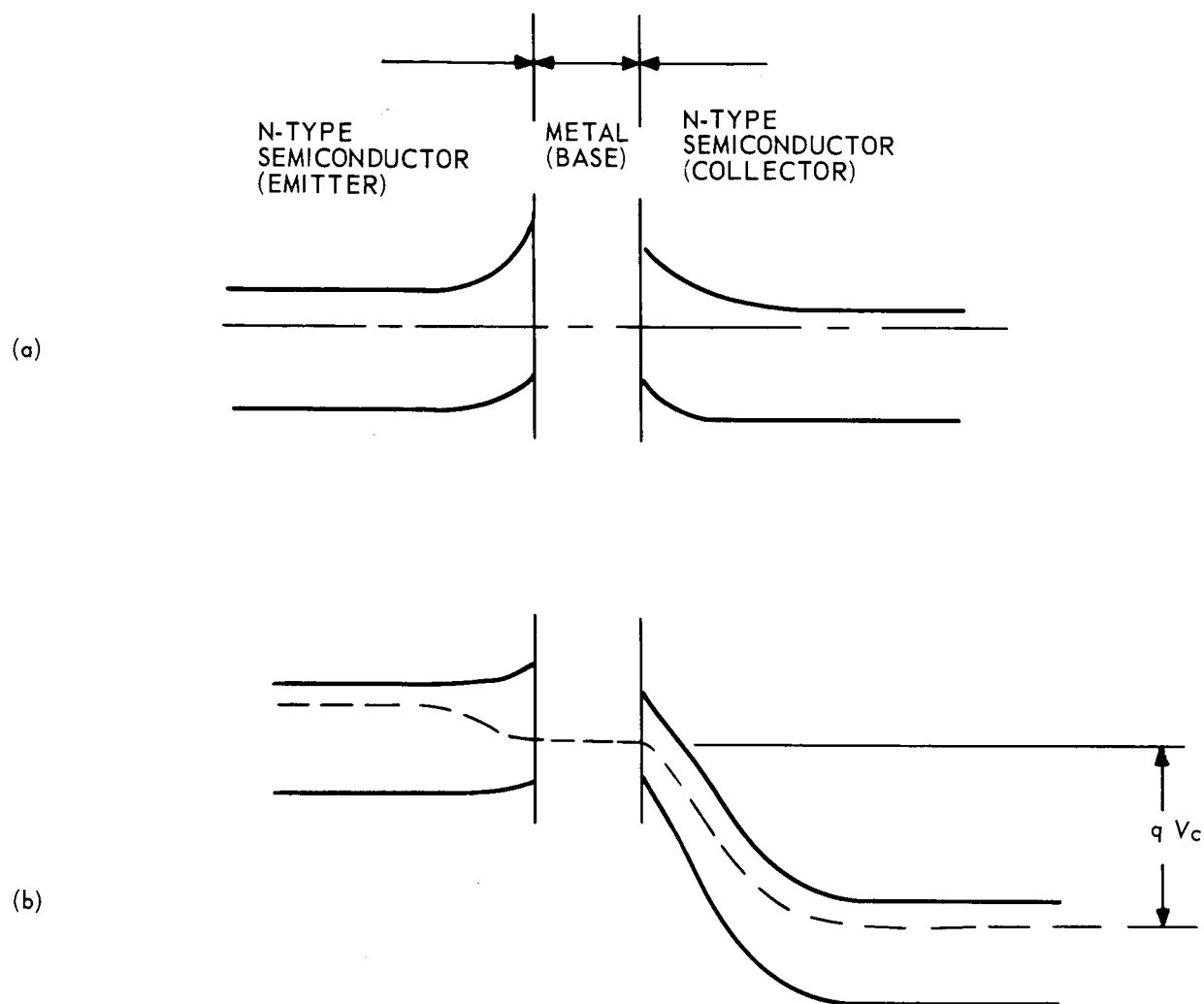
Figure 12. Energy Diagram of Metal Base Transistor (a) In Equilibrium,
(b) Under Operating (Biased) Conditions

The high-frequency behavior of the MBT can be evaluated by using the maximum frequency at which the gain of the device drops to unity, and is given by

$$F_{max} = \frac{\alpha}{4\pi} \left(\frac{1}{r_b C_c A_c \tau_{ec}} \right)^{1/2} \tag{1}$$

where:
α = common base current gain

r_b = base resistance

$C_c A_c$ = collector capacitance

τ_{ec} = emitter to collector delay time.

Comparing F_{max} of the MBT with that of the conventional bipolar transistor, it is expected that the MBT can have a F_{max} about an order of magnitude larger than the bipolar transistor. This anticipated performance can be arrived at if one considers two factors: (1) τ_{ec} for the MBT can be an order of magnitude samller than that for the bipolar transistor since the base transit time is negligible and only the emitter time constant is important. Hence, τ_{ec} for the bipolar transistor is given by the sum of τ_B (base transit time) and τ_e (emitter time constant). Hence, the improvement factor in τ_{ec} for the MBT is given by the ratio $\frac{\tau_e + \tau_B}{\tau_s}$, which can be as large as ten. (2) The base resistance (r_b) of the MBT, being a metallic layer, can be about an order of magnitude smaller than the base resistance of the bipolar transistor.

Since the MBT is a unipolar device (its operation being based solely on majority carriers), it does not require materials that have a high crystalline perfection. It is, thus, very suitable for fabrication by vacuum-deposition techniques.

35

Melpar's approach toward the fabrication of a thin-film MBT is as follows:

(1) To develop suitable metal-semiconductor junctions for eventual use as the emitter and collector junctions of the MBT. These junctions are to be in an all-evaporated structure suitable for incorporation into thin-film integrated circuits.

(2) To incorporate these junctions in an MBT structure and to study device feasibility.

(3) If device feasibility is demonstrated, and if the amplifier characteristics are encouraging, the effort will be directed toward high-frequency operation.

3.2 Material and Geometrical Considerations

3.2.1 Emitter and Collector Junctions

The energy bands of the materials used for the MBT must fit together as shown in figure 12. The barrier height of the emitter junction must be at least as high as the collector barrier, otherwise reflection of carriers will occur at the collector junction. This, in turn, will reduce the common base current gain, α.

The forward resistance of the emitter junction must be low for large power and voltage gain, while the reverse characteristics of the collector junction must be good (i.e., low leakage current, high peak inverse voltage, etc.). It is likewise important to deal with emitter-barrier heights of about 2 ev or less since the mean free path of electrons of energy greater than 2 ev in gold is less than 200Å.[23] At about 1 ev, the mean free path is reported to be about 740Å. Therefore, the lower the barrier heights with

36

which one can deal, the larger the mean free path of the electrons in the base region and, correspondingly, the larger the common base current gain.

A high-frequency design consideration (apart from using small areas for reduced capacitances) is the relative spacing of the emitter base and base collector. Two large a base-collector spacing relative to the emitter-base spacing might result in undesirable phase shifts between signal voltage and collector current. Hence, these spacings should be made approximately equal.

3.2.2 Base Region

A very important requirement for the efficient operation of the MBT is the effective transparency of the metal base layer to the injected carriers. Any losses incurred in the base region will reduce the gain of the amplifier. To reduce any losses in the base region due to phonon collisions, the base thickness should be made smaller than the mean free path of the carriers in the metal. At the present time, gold appears to be the most suitable for the base material. A gold film approximately 200 $\overset{o}{A}$ thick will transmit about 60 percent of the injected electrons. Another advantage of gold is its high conductivity. A 200 $\overset{o}{A}$ gold film has a sheet resistance of about 5 ohms/sq. This is important for high-frequency considerations.

The transmission of electrons through the thin metal base is given by

where:
$$\tau = (1-R) \, e^{-W/L}$$

τ = ratio of collected carriers to injected carriers

R = reflection coefficient at collector barrier

L = mean free paths of carriers in metal-base material

W = thickness of metal base.

Hence, for unity emitter efficiency (which is a reasonable approximation for the MBT since it is a unipolar device), the common base current gain, α, is given by equation (2). Hence, for large values of α, a small ratio of W/L is desired.

The base thickness for optimium frequency (gain bandwidth) design can be calculated as follows: The base resistance, r_b, is inversely proportional to the base thickness

$$r_b = \frac{k}{W} \tag{3}$$

where k is a function of the base resistivity and geometry. Combining equations (1), (2), and (3) results in

$$F_{max} = \frac{(1-R)}{4\pi} \left(\frac{1}{k C_c A_c \tau_{ec}} \right)^{1/2} (W^{1/2} e^{-W/L}) \tag{4}$$

which has a maximum at W=L/2. Hence, for optimum frequency design, the base thickness must be equal to half the electron mean free path in the base. The mean free path of electrons in gold has been reported for energies between 0.8 ev and 1.1 ev to be approximately 740Å. Hence, a base thickness of about 370Å is desired for optimium gain-bandwidth product.

3.3   Metal-semiconductor Junction Investigation

Thin-film structures (See figure 13 for geometry), suitable for both emitter and collector junctions, were fabricated by vacuum depositing compounds of zinc and cadmium selenide using gold electrodes. The energy-barrier height that exists between the gold plate and the semiconductor was

ISOLATION DIELECTRIC

EMITTER ELECTRODE

COLLECTOR ELECTRODE

E

C

EMITTER-BASE
SEMICONDUCTOR

BASE-COLLECTOR
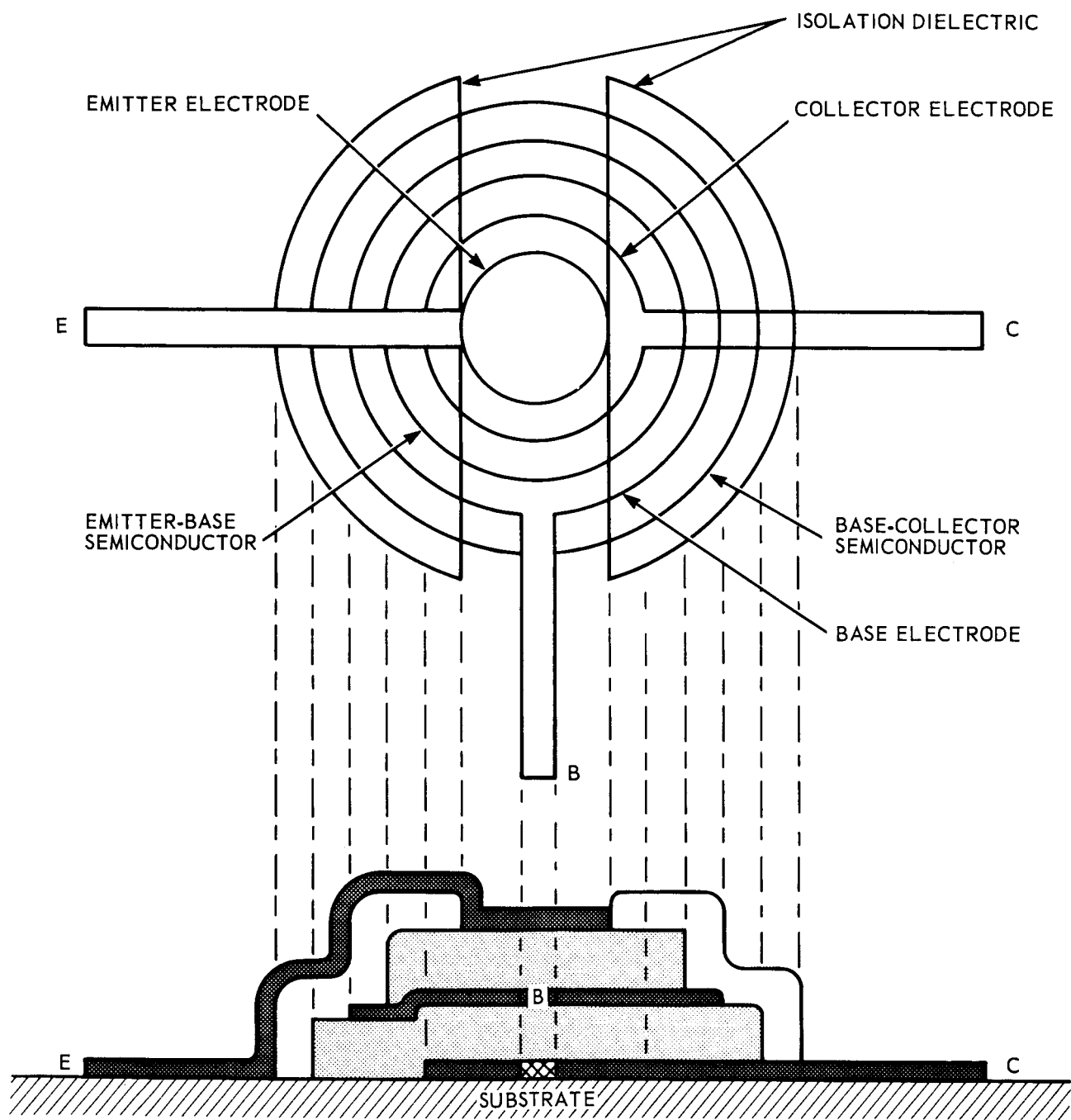SEMICONDUCTOR

BASE ELECTRODE

B

E

B

C

SUBSTRATE

Figure 13. Mask Layout and Deposition of MBT

found to be a function of the relative concentrations of the compounds, and could be varied from approximately 0.2 ev to 2 ev.

Figure 14 shows the I-V characteristics in room light of the first junction formed. A plot of ln I versus $\sqrt{V}$ (figure 15) shows that a Schottky-type barrier exists at the interface between the semiconductor system and the gold base electrode. This juntion exhibits a rectification ratio of about 2000 at 1 volt and a photovoltage of approximately 0.3 volt with a white light source approximately 1 inch from the sample. Although this junction exhibits a high forward resistance ($\approx4K\Omega$) and a low peak inverse voltage ($\approx3V$), it represents historically the first junction made with the above specified materials.

Figure 16 shows the I-V characteristics of a junction using the same materials with improvement in the deposition technique. This junction exhibits a peak inverse voltage of 6V, a forward breakdown voltage of about 0.4 volt, a forward resistance of about 200 ohms, and a rectification ratio of about 4×10^4 at 0.8 volt. The leakage current at a reverse bias of 4 volts is about one microamp. All the values given above were taken at room temperature. This junction shows the improvements over the first junction represented by figure 14, and indicates real progress during the initial quarter.

The junctions that are presently being fabricated exhibit rectification rations in the order of 10^5 to 10^6 at about 1 volt. The voltage-capacitance relationships, frequency response, etc. of these junctions have yet to be investigated at different temperatures and atmospheres.

I

V
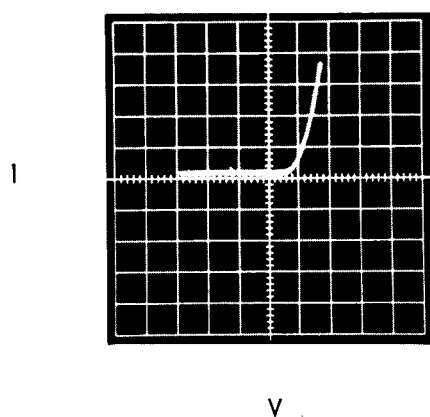
SCALE: VERTICAL - 0.05 ma/div
HORIZONTAL - 1 volt/div

Figure 14. I-V Characteristics of First Junction Fabricated

41
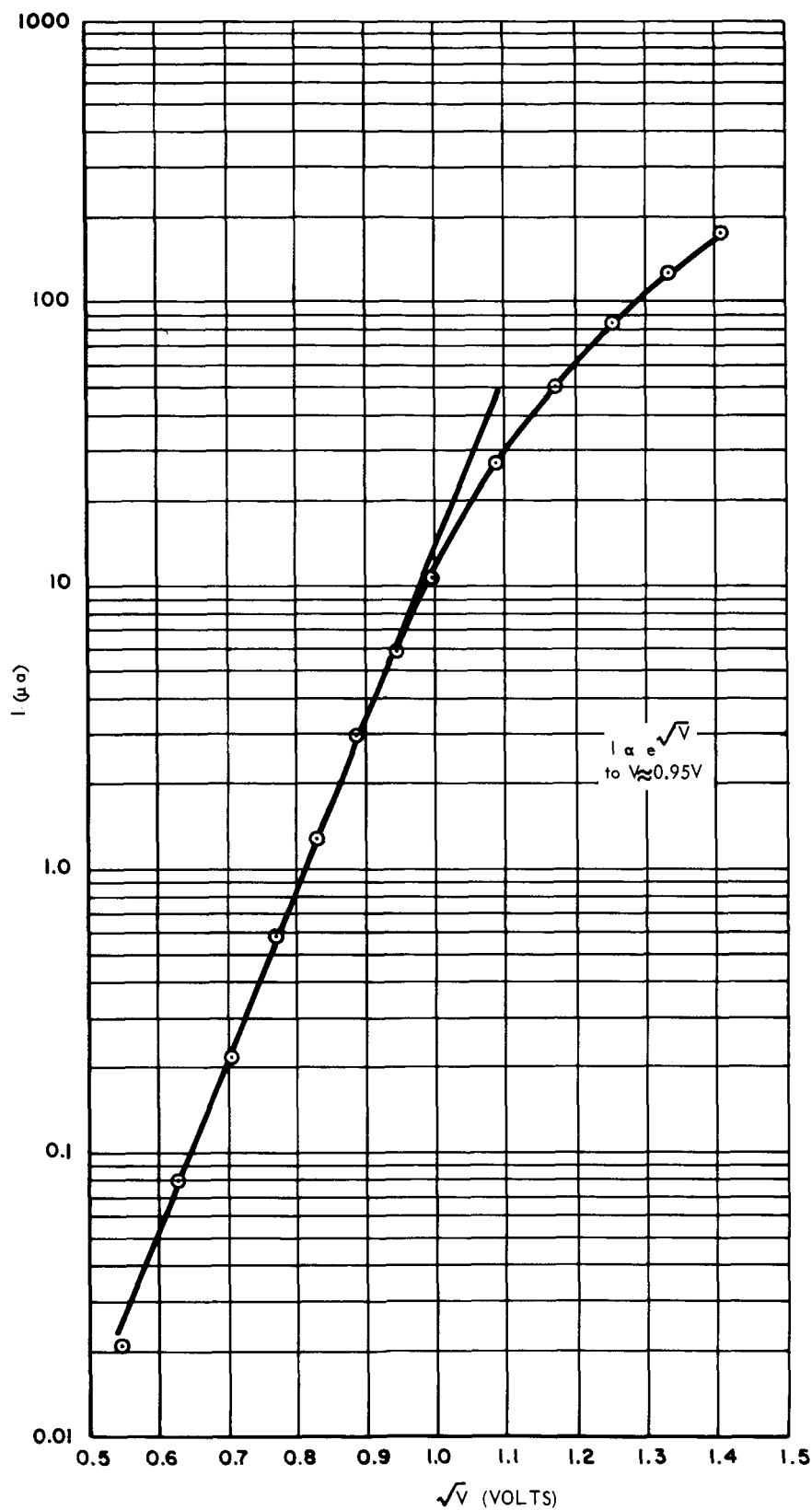
Figure 15. Plot of $\ln I$ vs. $\sqrt{V}$ for Junction of Figure 14 Measurements Taken in Dark

I

V
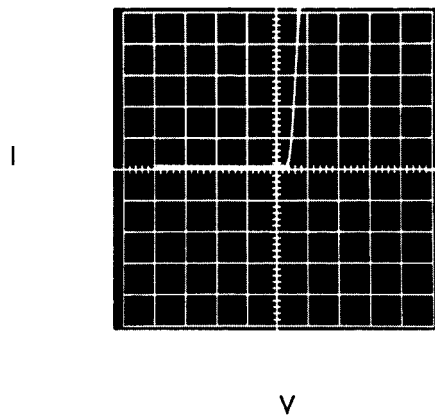
SCALE: VERTICAL - 0.5 ma/div
HORIZ. - 1 volt/div

Figure 16. I-V Characteristics of Improved Junction'

As of this report date, there have been no junction failures under shelf-life conditions. These junctions are unprotected, and are stored at room temperature and atmosphere. Their shelf and operating stabilities have been excellent.

A significant achievement in the junction work has been the ability to vary the potential barrier height and to position this barrier with respect to the electrodes. This is important since, in the MBT structure, one deals with "back-to-back" junctions with the proper relative energy barrier heights and levels.

The quality and characteristics of the deposited junctions provide strong encouragement for the realization of a thin-film metal base transistor.

4. HIGH-FREQUENCY SUBSTRATE INVESTIGATION

4.1 Substrate Evaluation

The choice of the best substrate for a particular thin-film application in the complete circuit function should be based on considerations of the following properties (in approximate order of importance):

(1) Surface topology

    (a) Smoothness

    (b) Flatness

    (c) Edge margin

(2) Compatibility with film materials

    (a) Adherence of the films to the substrate

    (b) Thermal expansivity

    (c) Chemical activity of substrate constituents

(3) Resistivity

    (a) Surface

        (i) Ultrahigh-frequency effective resistance

        (ii) Direct current

    (b) Volume

        (i) Direct current

(4) Dielectric constant

(5) Thermal conductivity

    (a) Thermal shock resistance

    (b) Dissipation of circuit heat

    (c) Attainment of thermal equilibrium

(6) Hygroscopicity

(7) Thermal stability

    (a) Retention of physical and chemical properties

    (b) Mechanical durability

Among those factors of lesser importance, but still to be considered, are
radiation resistance, cost and availability, transparency, and ease of cutting.

4.1.1 Surface Topology

    The surface characteristics of substrates are the most important
considerations in determining their usefulness of thin-film applications.
As far as the surface topology is concerned, one desires a surface which is
smooth, flat, and free of scratches and pits over its entire surface. There
is an "edge margin" around the perimeter of the substrate where the surface
is chipped, scratched, or pitted due to the cutting procedure. Thus, the
useful area of the substrate is within this margin, and one desires that
the edge margin be as small as possible. For most purposes, a smooth, pit-
and scratch-free surface finished to not more than 2 microinches is satis-
factory. The edge margin should not exceed 0.050 inch and the overall sub-
strate should be flat to 0.0005 microinch.

    Smoothness is extremely important to avoid failure of electrical in-
sulation by shorts or failure of resistors by open circuits (discontinuities).
Flatness is necessary so that the mask-to-substrate distance will be constant
and not too large. Large mask-to-substrate distance allows film material to
diffuse under the mask, often shorting closely spaced conductors, such as the
source-drain electrodes in the TFT. The edge margin must be known so that
the circuit can be laid out on the smooth, flat area within the margin.

4.1.2 Compatibility

By compatibility of the substrate with film materials we mean that:
(1) the various films must adhere well to the substrate, (2) the expansion
coefficient of the substrate closely resembles the mean of the expansivities
of the film materials, and (3) the substrates contain no impurities or
constituents which might react undesirably with film materials at normal
working temperatures. In general, the adherence between films and most
substrates currently in use is good, and no problem is foreseen in this
area. The matching of expansivities between film and a single substrate
is not possible for all thin-film materials, but substrates are available
in a variety of expansivities and the choice of substrate can be governed
by the expansivity of the film to be evaporated on it.

Spectrographic analysis, listing the impurities and constituents of
various substrates, is given in table I. The chemically active constituent
from which we might expect reactions with, for example, metal films, is
principally sodium. Sodium is present in all substrates studied, but in
varying quantities. The low-alkali-content substrates should be better
from the chemical-reactivity standpoint.

4.1.3 Resistivity

The surface resistivity, in general, less than the volume resistivity,
is of principal importance. Originally, it was thought that the ac surface
resistivity would be a major problem at high frequency in that a low surface
resistivity would, in effect, shunt the electrical components deposited on
its surface. However, the effective ac surface resistivity measured at 220
megacycles was found to be of the same order of magnitude for all substrates

Table I

SPECTROGRAPHIC ANALYSIS

Substrate sample	Aluminu	Barium	Boron	Calcium	Lead	Magnesium	Silicon	Sodium	Zinc
Corning 0211 (20 mil)	M	X	M	W	X	FT	VS	N	M
Corning 0211 (5 mil)	M	X	M	W	X	FT	VS	N	M
Corning 1723	M	M	M	N	X	N	VS	M	X
Corning 7059	N	N	M	W	X	FT	VS	W	X
Corning 7740	M	X	M	W	X	FT	VS	N	X
Corning 7900	W	X	M	M	X	W	VS	M	X
Corning 7940	W	X	FT	W	X	FT	VS	M	X
AlSiMag 614	VS	X	M	M	M	M	VS	M	X

Note: Concentration (%)

FT   0.001-0.005

W   0.01-0.5

M   0.5-4.0

N   4.0-5.0

VS   Major component

X   Searched, but not detected.

studied, so it is really not a deciding factor in the choice of substrate.
Figure 17 is the substrate test pattern for evaluating the effective ac
surface resistivity of 0.0005 squares at high frequencies. This is a
functional design for reducing inductance and lead length. The effective
reactance of the configuration was found to be capacitive with an average
capacitance of 0.9pf for high alumina substrates and 0.5pf for glass sub-
strates.

The measurement of the high-frequency characteristics was made with a
Boonton Radio Corp. Q-meter, Model 160-A, using the parallel-measurement
technique. For this method, one can calculate the effective parallel
resistance, R_p, from

$$R_p = \frac{Q_1 Q_2}{\omega C_1 \Delta Q} \tag{5}$$

the effective parallel reactance, X_p, from

$$X_p = \frac{1}{\omega(C_2 - C_1)} \tag{6}$$

and the effective parallel capacitance, C_p, from

$$C_p = C_1 - C_2. \tag{7}$$

The factors, Q_1 and C_1, are the Q and capacitance of the reference inductor
without the substrate connected to the measuring terminals; Q_2 and C_2 are
the Q and capacitance of the reference inductor and substrate connected in
parallel.

$$\Delta Q = Q_2 - Q_1$$
$$\omega = 2\pi f \tag{8}$$
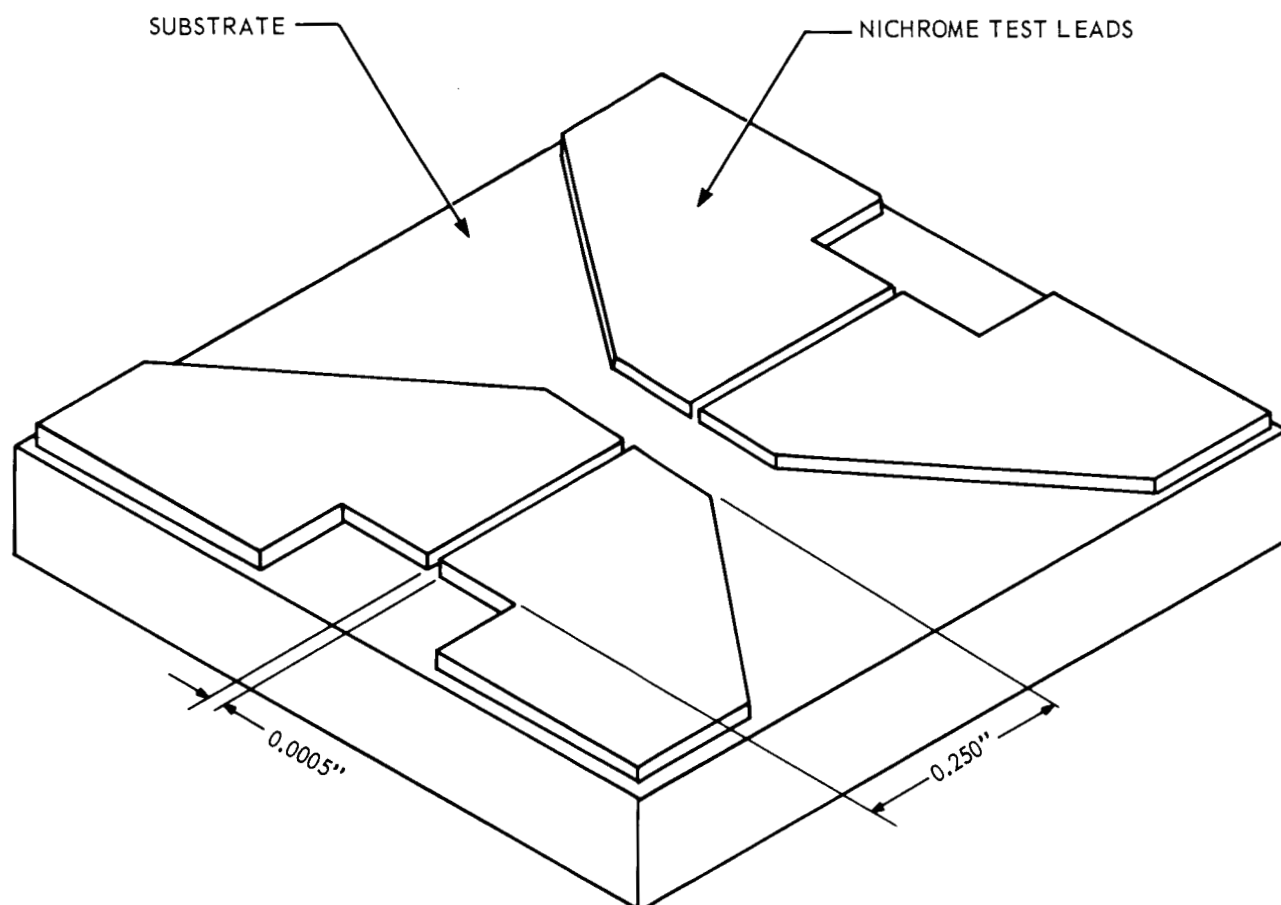
Figure 17. Substrate Surface Resistance Test Configuration for Measurements
at High Frequencies

The factor, f, is the measuring frequency of the Q-meter oscillator.

Note that, if the sign of (C_2-C_1) is negative (positive), the reactance is capacitive (inductive). Note also that, due to the fact that the effective parallel resistance is proportional to the products of the two Q values divided by the difference in Q values, a large error is introduced when equation 5 is used to calculate the effective surface resistance. Estimates of this error are of the order of 25%.

Figures 18 and 19 are curves of the effective series resistivity versus frequency for glass and basically alumina substrates respectively. Glass substrates appear to be slightly higher in surface resistivity than the high-alumina substrates.

A minature oven for measurements of the electrical properties of substrates at high frequencies and 100°C is shown in figure 20. The oven is designed to keep lead length short to reduce stray inductance and lead loss. The results of measurements of effective surface resistivity on Corning [R] code 0211 glass at room temperature and 100°C are shown in Figure 21. Note that there is very little effect on the properties of the substrate on temperature in this range. Note also that deviations from the presumed straight-line dependence of the resistivity on frequency are in the same direction for each frequency, even though the measurements at 100° and 32°C were made at separate times. The consistency in the error at each frequency suggests systematic error in the apparatus, which is amplified through the application of equation 5. A "best" fit of the data by the straight lines shown in figure 21 has the 32° line slightly above the 100°C line, which is to be expected, and is obvious since, in each case (with the exception
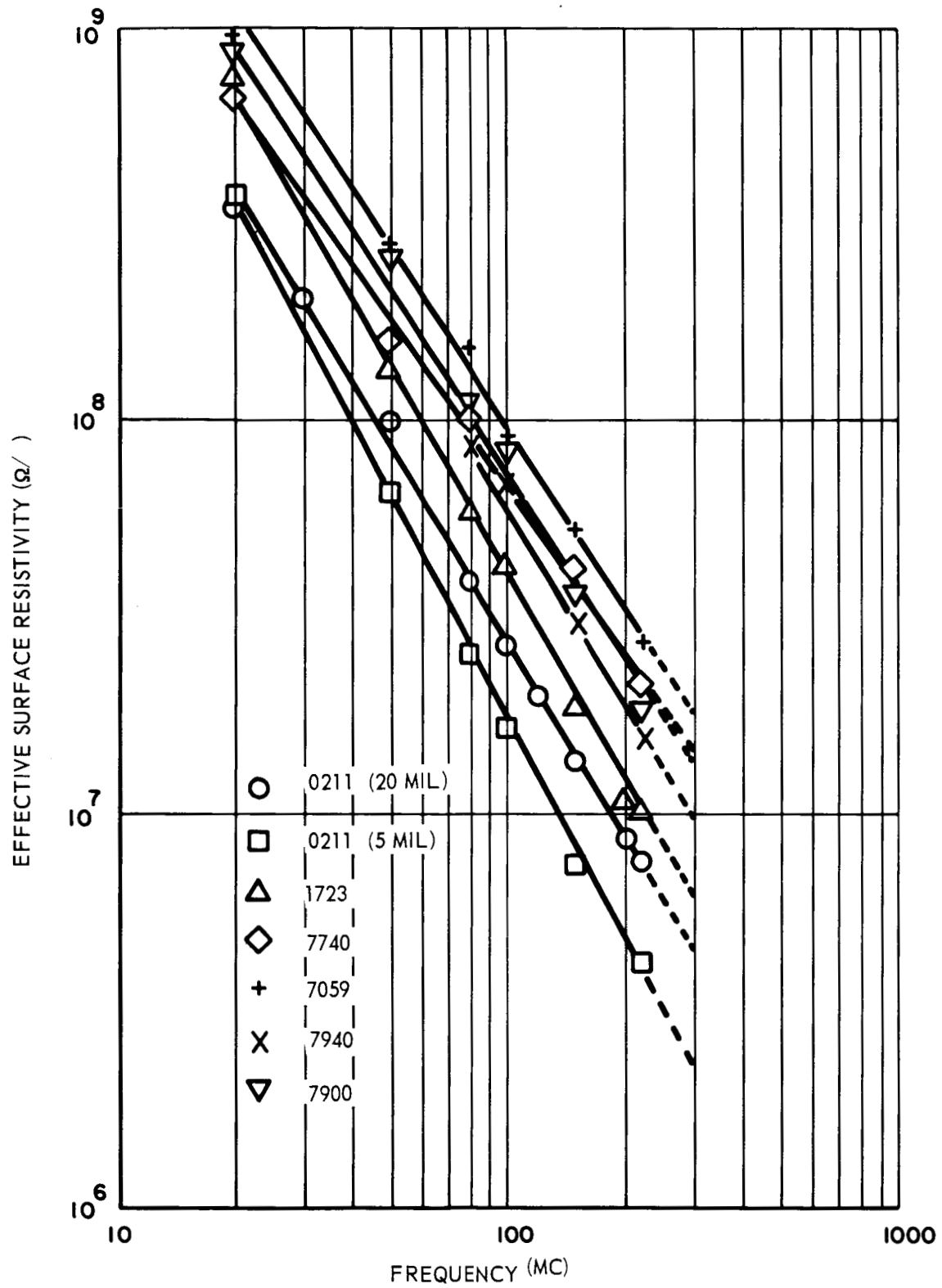
Figure 18. Frequency Dependence of Surface Resistivity of Several Glass Substrates
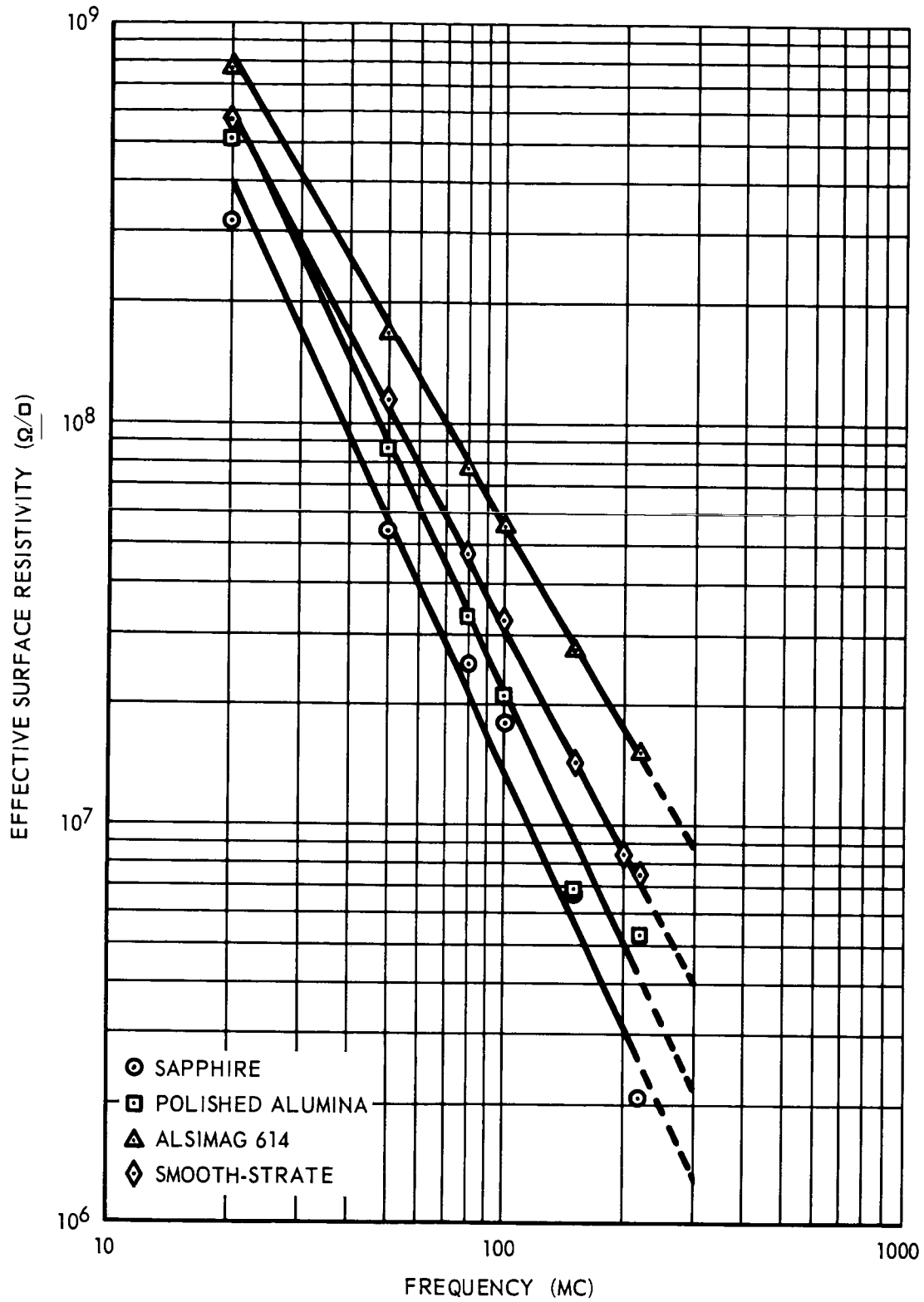
Figure 19. Frequency Dependence of Surface Resistivity of Several Basically Al_2O_3 Substrates

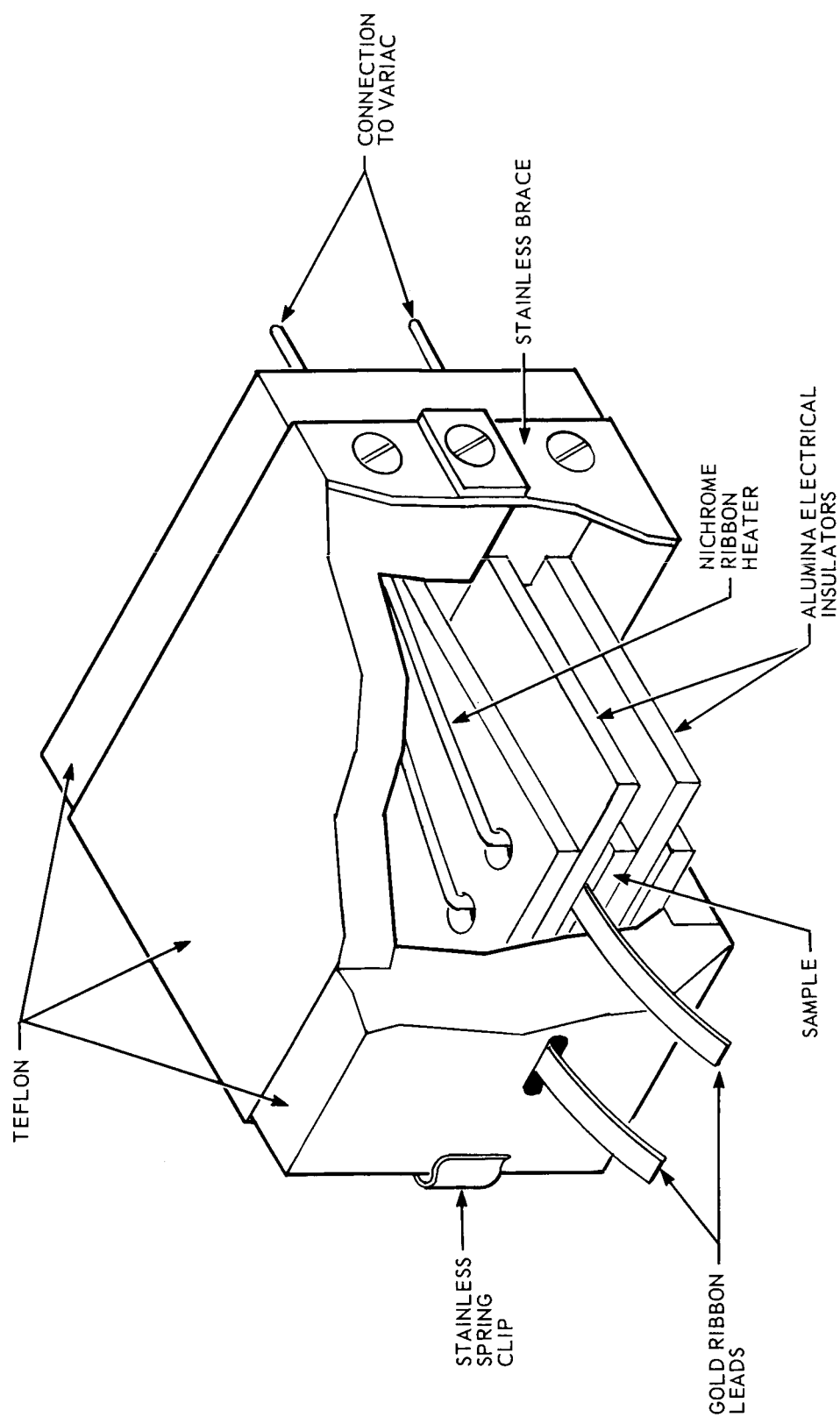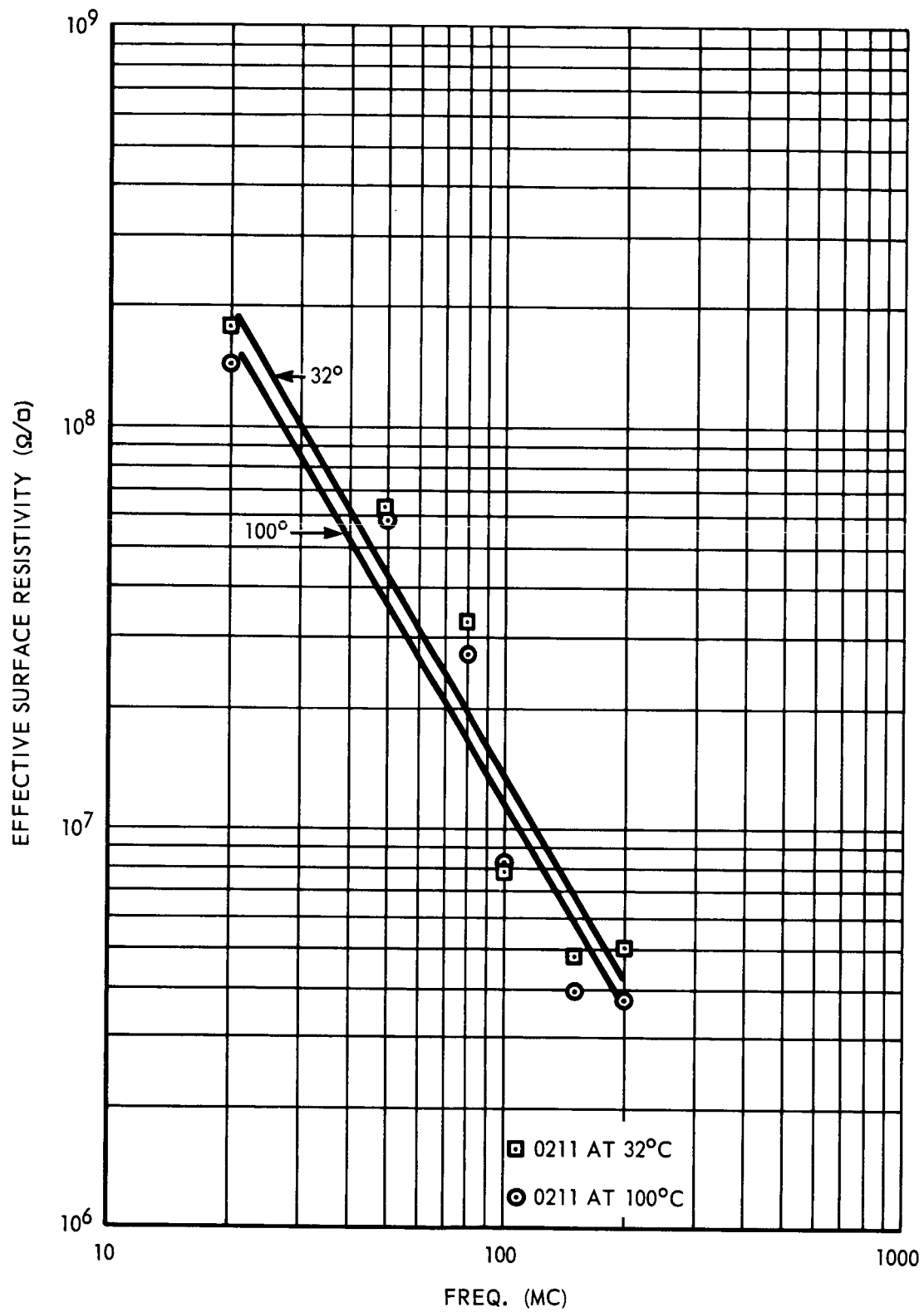Figure 20.   Miniature Oven for Heating Substrate to 100°C

Figure 21.   Frequency Dependence of Surface Resistivity of Corning[R] 0211 Substrates at Two Temperatures

of one), the value of the resistance at 32°C was higher that that at 100°C.

Due to the large error in calculation of the effective surface resistance of these substrates and the closeness of the effective resistance of all substrates, the surface resistivity will probably not be the deciding factor in choosing the "best substrate." Direct-current measurements of the surface resistivity will be tried next quarter in an effort to judge the relative worth of these substrates.

For certain applications, low-volume resistivity substrates, suitably passivated by an insulating film, might be useful. In general, however, high-volume resistivity substrates are more desirable to avoid stray capacitance and inductance, and such should be a criterion for choosing a suitable substrate.

4.1.4 Dielectric Constant

It is desirable to have the dielectric constant of a substrate as low as possible to help further reduce stray circuit capacitance.

4.1.5 Thermal Conductivity

Good thermal conductivity is necessary for thermal shock resistance, the dissipation of circuit heat, and the rapid attainment of thermal equilibrium. Often, processing of thin films requires rapid heating or cooling of the substrates. Substrates with low thermal conductivity tend to react to thermal shock or thermal gradients by shattering. The rapid dissipation of circuit or external heat to attain thermal equilibrium allows the circuit to stabilize more rapidly. Resistors operated at high power will necessarily heat up, and this heat must also be dissipated or damage can result to the resistor or adjacent circuitry.

4.1.6 Hygroscopicity

During the various clearing procedures, substrates come in frequent contact with aqueous solutions. As a standard procedure to remove adsorbed moisture and gases, the substrates are outgassed in vacuo immediately prior to the circuit evaporation. The degree to which the substrates are rid of the moisture and gases is proportional to the temperature and time of outgassing, and inversely proportional to the amount of gas or moisture adsorbed. A substrate which is porous or hygroscopic will adsorb larger amounts of water and will require more outgassing and, consequently, increase the time and cost of circuit fabrication. To keep outgassing time and temperature at a minimum, and avoid moisture damage to circuitry subsequent to fabrication, substrates should be chosen which are not hygroscopic.

4.1.7 Thermal Stability

The substrate must retain its physical, chemical, and mechanical properties over the wide temperature ranges of thin-film processing. Mechanical durability can be achieved if the strain point, annealing point, and softening point of the glasses are not exceeded in the processing of thin films. As indicated above, thermal conductivity has considerable influence on the mechanical durability also. We, of course, require that the electrical properties stay fairly constant with temperature so that the monitored components (resistors) are not affected by changes in the electrical properties of substrates with temperature. We are also concerned about the possible release of chemically active elements, such as sodium, from the glass structure which would tend to react with films or otherwise effect the substrate-surface properties.

4.2 General Considerations

There are numerous other factors which come into consideration such as cost, availability, reproducibility of properties, etc. Sectioning of circuits after formation requires that the substrates be easily cut. A substrate with low softening point seems to make welding leads to metal films easier and more reliable. Substrates should retain their properties under radiation. For some purposes, transparent substrates are more useful than opaque substrates, and vice versa. Thus, there are many considerations in choosing a substrate, and one universal substrate will probably never be found which will be completely satisfactory for all purposes.

4.3 Cumulative Data

Some of the properties of considerable importance for various substrates are listed in table II. The smoothness values given here are those quoted by the manufacturers. The values listed for the flatness were measured using an Ames Co. dialatometer, which can measure variations to 0.0001 inch. The values are the maximum variations in thickness since the dialatometer reads the distance from the back of the substrate to the front surface of the substrate. If the two surfaces are not parallel, this discrepancy will be added on to the variations across one surface. Thus, we can say the flatness is less than the figures given in table II. The ac resistivity was measured as described above. The values given are extrapolations of the lines representing "best fit" to 300 megacycles. The expansivities and softening points are those values quoted by the manufacturers.

Table II

CUMULATIVE DATA

Substrate mfg and code No.	Description	Surface resistivity @300 mc (Ω/sq)	Smoothness (μ-inch)	Flatness (inch/inch)	Expansivity ($^\circ$C)$^{-1}$	Softening Point ($^\circ$C)
(1) Corning 0211 (Microsheet)	Alkali-zinc borosilicate class	4.5×10^6	< 0.25	$< \pm .0004$	7.2×10^{-6}	720
(2) Corning 1723 (Alkali free)	Lime alumino-silicate glass	6.0×10^6	----	$< \pm .0002$	4.6×10^{-6}	912
(3) Corning 7059 (Pyrex (R)) (Alkali free)	Barium alumino Silicate glass	1.8×10^7	< 0.25	$< \pm .0004$	4.5×10^{-6}	872
(4) Corning 7740 (Pyres (R))	Alkali boro-silicate glass	1.45×10^7	----	$< \pm .0002$	3.25×10^{-6}	820
(5) Corning 7900 (Vycor (R))	96% silica boro-silicate glass	1.35×10^7	----	$< \pm .00005$	8.0×10^{-7}	1500
(6) Corning 7940 (Alkali free)	Fused silica	9.8×10^6	----	$< \pm .00055$	5.6×10^{-7}	1580
(7) Insaco Inc. (Linde) Sapphire	Single crystal Al$_2$O$_3$	1.3×10^6	< 5.0	$< \pm .00055$	8.7×10^6	----
(8) AlSiMag (R) 753	Polished alumina ceramic	2.2×10^6	< 20.0	$< \pm .00018$	6×10^{-6}	1650

Table II (Continued)

Substrate mfg and code No.	Description	Surface resistivity @300 mc (Ω/sq)	Smoothness (μ-inch)	Flatness (inch/inch)	Expansivity $(^\circ C)^{-1}$	Softening Point $(^\circ C)$
(9) Electroceramics Smooth-Strate (R)	Alkali-free, glazed alumina ceramic	4.0×10^6	<0.5	$<\pm.00052$	6.65×10^{-6}	1816
(10) AlSiMag (R) 614	Glazed alumina ceramic	8.7×10^6	Scratches prominent	$\pm.0015$	6.4×10^{-6}	1550

Note: (R) = Registered trademark.

4.4 Conclusions

Some tentative conclusions can be noted at this time. They are:

(1) Drawn glasses, in which group Corning 0211 and 7059 are classified, are smoother and cost less than those which require grinding and polishing. Nondrawn glasses require an extra process of cutting and polishing, and hence cost more.

(2) Ground glasses seem to be flatter, however, this factor of approximately two increases in flatness does not delete the disadvantage in lack of smoothness.

(3) Code 7059 has a higher effective ac surface resistivity and lower alkali content, and is preferred for this reason over Code 0211 glass.

(4) For some experimental purposes, the use of code 0211 glass may be warranted since its cost is considerably less than code 7059.

(5) The best high-alumina substrate found to date is Smooth-Strate.[R] It has the best surface topology and is advertised as being alkali free.

(6) AlSiMag 614 was found to be totally unacceptable for our purposes because of both high alkali content and poor surface topology.

5.   DIELECTRIC INVESTIGATION

The physical geometry of a capacitor has considerable effect on its electrical properties at high frequencies. A capacitor is actually a short length of "strip" transmission line with infinite load impedance. This can be seen from the definition of a general transmission line, which is any system of separate current-carrying conductors having a potential between them. The distributed parameters of any transmission line can be represented by the lumped constants r (resistance), c (capacitance), l (inductance), and g (conductance) per unit length. These constants are shown in figure 22. The rate of change of voltage with respect to distance down the line is found experimentally to be equal to the current times a constant, z, equal to the impedance per unit length.

$$\frac{dV}{dx} = zI. \tag{9}$$

It is, likewise, noted that

$$\frac{dI}{dx} = yV \tag{10}$$

where y is called the admittance per unit length.

It can be shown that
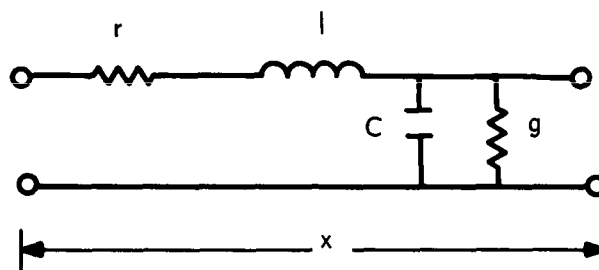
$$z = r+jwl \tag{11}$$

and

$$y = g+jwc. \tag{12}$$

The quantity $\sqrt{z/y}$ becomes important in transmission-line calculations and is

NASA HOUSTON QUARTERLY

DISTRIBUTED PARAMETERS OF A SECTION
OF TRANSMISSION LINE OF LENGTH X

Figure 22. Distributed Parameter of Section of Transmission Line of Length X

given the name <u>characteristic impedance</u>, Z_o

$$Z_o = \sqrt{\frac{z}{y}} \quad .$$
(13)

Substituting equations 11 and 12 into equation 13 and considering only high

frequencies

$$Z_o = \sqrt{\frac{l}{c}} \quad .$$
(14)

Another quantity of considerable importance is the <u>propagation</u>

<u>constant</u>, defined

$$\gamma = \sqrt{zy} = \alpha + j\beta$$
(15)

where substitution at high frequencies gives

$$\alpha = \frac{lg+rc}{2\sqrt{lc}} \quad , \quad \beta = \sqrt{lc} \quad .$$
(16)

One can show 24 the velocity of phase propagation

$$V = \frac{\omega}{\beta} = \frac{}{\sqrt{lc}} \quad .$$
(17)

where lc (henrys farads m^{-2}) $= 0.113 \times 10^{-16} \epsilon_r(d) \mu_r(d)$, and $\epsilon_r(d)$ and $\mu_r(d)$

are the relative dielectric constants and dielectric permeabilities of the

insulator between the conductors. The wavelength, λ_g, in the line of a wave

whose wavelength in air is $_o$ is given as

$$\lambda_g = \lambda_o \frac{V}{C_o}$$
(18)

where C_c is the velocity of light in air.

Thus, from equations 17 and 18,

$$\lambda_g = \frac{\lambda_o}{C_o \sqrt{lc}} = \frac{\lambda_o}{C_o} \frac{}{\sqrt{0.113 \times 10^{-16} \epsilon_r(d) \mu_r(d)}} \quad .$$

Choosing practical values for these constants, for a 300-megacycle

wave,

$$\frac{\lambda_o}{C_o} = \frac{1}{V_o} = \frac{1}{300 \times 10^6} \quad (\text{sec})$$

$$\varepsilon_r(d) = 4.5 \text{ and } \mu_r(d) = 1.0$$

and, thus,

$$\lambda_g = 47.3 \text{ centimeters}$$

for the wavelength of a 300.mc wave in the transmission line.

Now, for an open-circuited transmission line whose length is less than a $\lambda_g/4$, the transmission line behaves as a capacitor. If the line length is greater than $\lambda_g/4$, it behaves as an inductor.[25] Thus, the capacitor must be less than

$$\frac{\lambda_g}{4} \quad 12 \text{ centimeters}$$

to behave like a capacitor at 300 megacycles. This is not a stringent requirement on capacitor geometry for thin-film circuitry. Thus, at least theoretically, there appears to be no problem in having a capacitor retain its capacitive characteristics at 300 megacycles.

6. INDUCTORS

6.1 Inductance

Flat, spiraling, square coils provide the highest area efficiency and lowest intercoil capacitance, with the simplest masking technique. The empirical formula developed by Bryan[26] for printed circuits is

$$L = .141 \, an^{5/3} \log 8\frac{a}{c}$$

where: n = number of turns

$$a = \frac{A + B}{4} \text{ (inches)}$$

$$c = \frac{A - B}{4} \text{ (inches)}.$$

A is the overall outside square length and B is the inside square length of a corresponding side of the inner area (where the coil has not been deposited). The a/c ratio can be selected for maximum Q or maximum L or, as is usually the case, some compromise value.

The inductance can be increased by enclosing the coil with a high-resistance ferrite or an insulated iron deposition. This technique increases the inductance by a factor equal to the magnetic permeability of the material. In practice, the increase in inductance is not as large as expected from the theory because the coupling in a flat coil is very inefficient, and the high bulk permeability value of iron or ferrite has not yet been realized in thin-film form. However, these methods of increasing inductance would be preferable to simply increasing the area because a flat coil without any close-coupling magnetic material radiates much more electromagnetic wave energy than the standard inductor with its greater mutual coupling. Thus, the larger the flat-coil area, the greater the circuit-shielding problem.

6.2 Self-resonance

Self-resonance is the effect when the coil, without any external cap-
acitance, resonates with its own capacitance between conductors, with either
ari or the substrate for a dielectric. The theoretical calculation for the
self-resonant frequency (f_o) of these coils is[27]

$$f_o = \frac{c}{4 \ell \sqrt{\epsilon_r}}$$

where: c = velocity of light in free space

ℓ = coil length

ϵ_r = substrate dielectric constant.

This formula considers the coil as a quarter wavelength shorted transmission
line. Also, the coil, being flat, is considered a current sheet which
affects the current concentration.

The equivalent coil capacitance (c) can then be calculated using the
tank circuit resonance equation

$$f_o = \frac{1}{2\pi\sqrt{LC}}$$

6.3 Inductor, Q

The natural resonant frequency of a coil must be much greater than
the desired circuit frequency used if high Qs are to be achieved.

The conductor resistance of the coil is the major limitation on Q.
The inductor, Q, equation is

$$Q = \frac{2\pi f L}{R_{coil}}$$

f = frequency (cycles per second)

R = coil resistance (ohms)

L = inductance (henries).

That is to say that Q is equal to the ratio of the ac impedance of the inductor divided by the resistance. This resistance at low frequencies is the dc resistance, but changes (increases) at high frequencies because of a phenomenon called the skin effect. The skin effect is due to the fact that, as the frequency increases, the current in the conductor becomes more and more concentrated in the outer edges so that, for example, at very high frequencies, a solid circular conductor could be replaced by a hollow cylinder as long as the cylinder walls were as thick as the skin depth at that frequency.[28]

$$d = \frac{1}{\sqrt{\pi f \mu \sigma}}$$

d = skin depth (meters)

f = frequency (cycles per second)

μ = permeability (henry per meter)

σ = conductivity (mho per meter)

The skin depth (d) is the depth at which the electric field, magnetic field, and current density are all equal to 1/e of their respective values at the conductor surface.

6.4 Deposition Techniques

Three-mil molybdenum masks were used to form inductors in two steps. The first mask formed horizontal conductors and the second mask formed the interconnecting vertical conductors to complete a flat, spiraling, square coil.

The first deposition was 500 angstroms of chromium for adherence to the substrate and then copper was deposited over the chromium for low resistivity.

The copper thickness was approximately 26,000 angstroms.

6.5 Deposited Inductors

The characteristics of the inductors, theoretical and actual, are given in table III. The actual values were obtained using the Boonton, 190-A, Q meter.

Two types of substrates were used, Corning 0211 alkali zinc borosilicate glass and Englehard quartz.

6.5.1 Inductance Values

The empirical formula developed by Bryan[26] for printed circuits resulted in excellent predictions on three of the five inductors. The other two certainly could be considered "ball-park" values. Since the actually obtained values seem to be very repeatable, if necessary, another empirical formula could be developed for a particular type of inductor.

6.5.2 Self-resonant Values

The discrepency between the calculated values of inductor self-resonant frequency and the actual value were not unexpected. The reason for this difference is due to the fact that the calculation involves using the velocity of light in free space. In actuality, the electric field travles slower in a conductive medium such as copper. The ratios of f_o actual to f_o theoretical yield values ranging from 0.52 to 0.75. As a comparison, the typical value of this "velocity factor" for shielded cable is 0.66.

The dielectric constant of the glass and quartz differs with the result that the lower dielectric constant of quartz should give a higher self-resonant frequency. The actual differences in these values are well within the experimental error of the measurements and, therefore, there seems to be

Table III

INDUCTOR VALUES

Substrate	Conductor width (mils)	Space (mils)	Outer diameter (inches)	Inner diameter (inches)
1	10	10	0.4	0
2	25	25	0.8	0
3	35	15	0.8	0
4	15	35	0.8	0
5	10	10	0.6	0

Substrate	Theoretical $L(\mu h)$	Theoretical f_o(mc)	Actual $L(\mu h)$	Actual f_o(mc)	Q (30 mc)	$\frac{f_o \text{ actual}}{f_o \text{ theoretical}}$
1A	0.392	168	0.498	86	4.3	0.52
1B	0.392	168	0.487	86.8	8	0.52
2A	0.544	105	0.555	77.7	6.9	0.74
2B	0.544	105	0.602	74.7	11.5	0.71
3A	0.544	105	0.527	79	8	0.75
3B	0.544	105	0.569	76.9	12	0.73
4A	0.544	105	0.615	75.2	5	0.72
4B	0.544	105	0.664	71.7	9.2	0.68
5A	1.15	74.5	1.47	49.8	5	0.67
5B	1.15	74.5	1.56	48.2	6.4	0.65

A = Corning 0211 glass substrate.

B = Englehard quartz substrate.